Aerodynamic Model Identification of the Flying V from Sub-Scale Flight Test Data

Ruiz Garcia, A.; Brown, M.T.H.; Atherstone, D.M.; van Arnhem, N.; Vos, Roelof

DOI
10.2514/6.2022-0713

Publication date
2022

Document Version
Final published version

Published in
AIAA SCITECH 2022 Forum

AIAA SciTech Forum
January 3-7, 2022, San Diego, CA & Virtual
AIAA SCITECH 2022 Forum

10.2514/6.2022-0713

Aerodynamic Model Identification of the Flying V from Sub-Scale Flight Test Data

Alberto Ruiz García*, Malcom Brown†, Daniel Atherstone‡, Nando van Arnhem§, and Roelof Vos¶
Delft University of Technology, Delft, 2629 HS, The Netherlands

This paper presents the identification of the aerodynamic model of the "Flying-V", a novel aircraft configuration. The aerodynamic model is estimated using flight test data from a 4.6% sub-scale model. The dataset includes longitudinal and lateral-directional maneuvers performed by both the pilot and the autopilot to excite the aircraft dynamic modes. The so-called Two-Step Method is used to decouple and simplify the aerodynamic identification problem; the state estimation step is performed by an Iterated Extended Kalman Filter, and the parameter-estimation step using ordinary least squares. A stepwise regression technique and previous knowledge from wind-tunnel tests are combined to select the model structure, and the identified model is validated using a third of the gathered data. The estimated models are parsimonious and considered adequate in terms of model fit, with a maximum relative Root Mean Square Error of 10% for the worst validation case. For the considered location of the center of gravity and flight conditions, the estimated aerodynamic derivatives confirm that the aircraft is longitudinally stable, both statically and dynamically; and that it is also laterally and directionally statically stable. The analysis of the dynamic modes of the sub-scale model showed stable short period and roll subsidence modes, a lightly damped Dutch roll mode, and lightly damped/unstable phugoid and spiral modes.

Nomenclature

Latin Symbols

b	Wingspan, [m]
$\bar{c}$	Mean Aerodynamic Chord, [m]
C_X, C_Y, C_Z	Force coefficients in body axes, [-]
C_l, C_m, C_n	Moment coefficients in body axes, [-]
$C_{\alpha,up}$	Upwash coefficient at probe location [-]
G	Orthogonalization matrix
J	OLS cost function, advance ratio [-]
L, M, N	Roll, pitch and yaw moment, [N·m]
m	Mass, [kg]
n	Number of regressors in model
N	Number of samples
p, q, r	Angular body rates [rad/s]
$\hat{p}, \hat{q}, \hat{r}$	Dimensionless angular rates [-]
$\mathbf{p}_j$	Regressors, $j = 1, 2, ..., n$
q_∞	Dynamic pressure, [kg·m/s^2]
$\mathbf{r}$	Residual vector
S	Reference area, [m^2]
$\mathbf{t}$	time
$\mathbf{u}$	Control vector
u, v, w	Body velocities [m/s]
v	Measurement noise
V	True airspeed, [m/s]
w	Process noise
W_{xE}	Wind speed in North direction [m/s]
W_{yE}	Wind speed in East direction [m/s]
$\mathbf{x}$	State vector
X	Regression matrix
X, Y, Z	Aerodynamic forces in body axes, [N]
$\mathbf{y}$	Dependent variable
$\mathbf{z}$	Measurement vector

Greek Symbols

α	Angle-of-attack, [deg, rad]
β	Angle-of-sideslip, [deg, rad]
χ	Aerodynamic state vector

*PhD candidate, Faculty of Aerospace Engineering, A.RuizGarcia-1@tudelft.nl, AIAA student member.
†Graduate researcher, Faculty of Aerospace Engineering.
‡Graduate researcher, Faculty of Aerospace Engineering.
§PhD candidate, Faculty of Aerospace Engineering, AIAA member, pilot Flying-V.
¶Assistant Professor, Faculty of Aerospace Engineering, Associate Fellow AIAA.

δ_a	Aileron deflection [deg, rad]
δ_e	Elevator deflection [deg, rad]
δ_r	Rudder deflection [deg, rad]
$\boldsymbol{\lambda}$	Bias vector [m/s^2, rad/s]
ϕ	Roll angle [rad/s]
ψ	Yaw angle [rad/s]
ρ	Air density [kg/m^3]
θ	Pitch angle [rad/s]
$\boldsymbol{\theta}$	Parameter vector
$\boldsymbol{\xi}_j$	Orthogonal regressors, $j = 1, 2, ..., n$

Subscripts

acc	accelerometer
aug	augmented
e	engine
E	Earth-fixed reference frame (NED)
m	measured
probe	referred to air data probe
$X,\ Y,\ Z$	Body axes reference frame
$i,\ j$	integers

Acronyms

ARMAX	Auto-Regressive Moving Average with eXogeneous inputs
BLUE	Best Linear Unbiased Estimator
DADC	Digital Air Data Computer
CAD	Computer Aided Design
CFD	Computational Fluid Dynamics
IEKF	Iterated Extended Kalman Filter
MAC	Mean Aerodynamic Chord
OJF	Open Jet Facility
OLS	Ordinary Least Squares
PRESS	Predicted Residual Error Sum of Squares
RMS	Root Mean Square Error
SVD	Singular Value Decomposition
TSM	Two-Step Method
VIF	Variance Inflation Factors

I. Introduction

With the aim of reducing the global-warming impact of large, long-range transport aircraft, a new aircraft configuration was proposed in 2015 [1], named "Flying V". It is a highly swept flying-wing aircraft with the passenger cabin located inside the wing. Initial studies carried out at Airbus suggested that the Flying V could theoretically outperform the Airbus A350 by 10% in terms of aerodynamic efficiency, while having a slightly lower operating empty weight. An optimization of the planform geometry and the aerodynamic shape was done in Ref. [2], estimating the lift to drag ratio of the aircraft for cruise conditions to 23.5. A concurrent study on the same geometry, in conjunction with Airbus, showed a double-digit reduction in structural weight fraction compared to a reference aircraft [3, 4]. In Ref. [5] the installation effects of over-the-wing turbofan engines on the Flying V were investigated, concluding that engine location plays an important role in the aircraft lift-to-drag-ratio, leading to penalties up to 10% compared to the engine-off configuration. A recent study into the conceptual design of a three-member family of Flying-V aircraft has shown a 20% reduction in fuel use over the design range of 15,000km [6]. An artist impression of the Flying V is shown in Fig. 1.

A number of experiments have been performed on a 4.6%-scale wind-tunnel test article of the Flying V, at a Reynolds number based on the mean aerodynamic chord of 1 million. Using this test article, an untrimmed maximum lift coefficient of 1.02 was demonstrated, as well as an aerodynamic center excursion over angle-of-attack as much as 55%$\bar{c}$ due to vortex formation on the suction side of the wing, and a trimmed maximum lift coefficient of 0.68 [7]. In Ref. [8] a global longitudinal aerodynamic model was derived by applying system identification techniques to the static wind tunnel data. The resulting model was used for trim and take-off calculations before the first flight of the sub-scale model described in Section II and is the starting point of the present study. The effect of engine integration on the aerodynamic interference was studied experimentally in Ref. [9]. It was shown that the interference effects on lift and pitching moment were of the same order of magnitude as the effect of superpositioning the contributions of the isolated wing and engine. The effect of the winglet and rudder integration on the aerodynamic coefficients was studied in Ref. [10], showing a strong reduction in yawing-moment-due-to-rudder-deflection with increasing angle of attack. Finally, in Ref. [11] it was determined that the addition of fences and vortilons has little effect on the pitch break that occurs at an angle-of-attack of 20°.

While the static wind-tunnel tests provide further insight into the aerodynamic characteristics of the Flying V, it does not reveal anything about the dynamic aerodynamic derivatives, which are key to assess the handling qualities and further development of a flight control system for such an unconventional configuration.. Furthermore, the half-model setup in an open wind tunnel comes with its own challenges in terms of corrections that need to be applied to correlate the aerodynamic coefficients to a full-span free-flying airplane. Finally, if

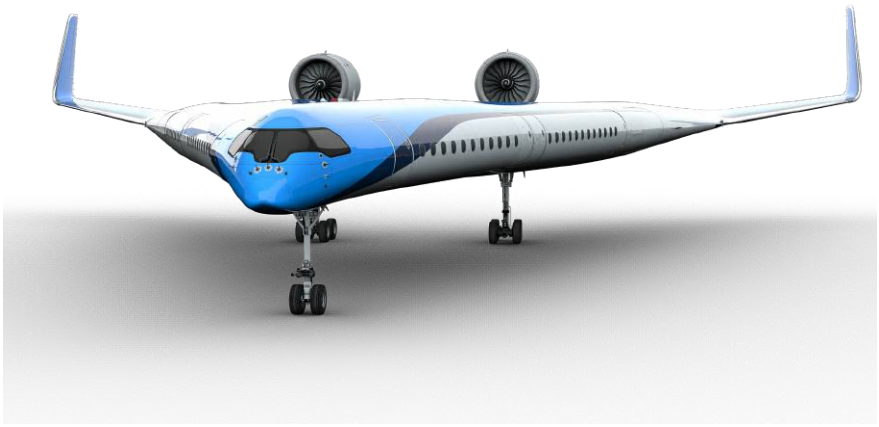

Fig. 1 Artist impression of the Flying V, a long-haul passenger aircraft, seating more than 300 passengers in a standard two-class configuration.

one wishes to assess the handling qualities of such an unconventional airplane, also the inertia properties are to be taken into account in addition to the flight control laws. Therefore, the goal of this study is to identify the global aerodynamic model of a 4.6%-scale test article of the Flying V through a free-flight experiment and to use this model to identify the longitudinal and lateral-directional eigenmodes of this airplane. The reader should be reminded that the outcomes of this study refer to a sub-scale model that operates at low Reynolds number. This study should therefore be interpreted as a starting point of further studies on the full-scale version.

The identification of an aerodynamic model from flight test data can be considered as a joint state-parameter estimation problem [12]. The variables required for the aerodynamic parameter estimation are measured during the flight or can be determined from the measurements. However, they include measurement bias and noise, so the actual values need to be estimated before they can be used in the parameter estimation. This coupled identification problem can be solved using output-error methods, which are nonlinear optimizations that estimate the aircraft states and the parameters of the aerodynamic model in a single step. This approach has been widely used in the past for aircraft system identification, where the absence of process noise is a reasonable assumption if the atmosphere is calm[13–15]. Process noise is seldom included since its treatment is considerably more complex, requiring a filter-error method instead. Filter-error methods have been used to model atmospheric turbulence as additional noise in the states, which makes them stochastic variables[16].

These methods are complex and may suffer from convergence problems when a large number of unknown parameters are involved[17], which is the case in aircraft model identification since one usually needs to estimate instrument biases, wind speeds, and the parameters of the aerodynamic model. A simplification of the joint state-parameter estimation problem for aircraft called the *Two-Step Method* (TSM) was first developed at Delft University of Technology in the 1970's [18] and has been successfully used in various aircraft system identification studies[12, 19–21].

The main feature of the Two-Step method is the decomposition of the joint state-parameter estimation problem into two simpler ones: a state estimation problem (flight path reconstruction) and a parameter estimation problem. The flight path reconstruction involves the nonlinear equations of motion and it is performed using a nonlinear Kalman filter. Examples can be found using an Extended Kalman Filter (EKF)[19], an Iterated Extended Kalman Filter (IEKF)[20], or an Unscented Kalman Filter (UKF)[21].

To determine an adequate model structure, or in other words, to select which variables should be included in the model, a stepwise regression technique can be used. This iterative routine is relatively simple to implement and has been used successfully in the past for aircraft system identification purposes [22–25]. An adequate model structure for the Flying V from static wind-tunnel data was found using this technique [8], so it is chosen as the model structure determination method adding some ideas from the work of Ulbrich [26, 27]. More complex estimation methods such as B-splines[28, 29], Multivariate Simplex Splines[30], or Neural Networks[31] are deemed unnecessary at this stage since the aerodynamic forces and moments at the tested

conditions can be properly captured by simpler models.

The paper is structured as follows. The research vehicle and instrumentation used during the tests are described in Section II. The methodology to perform the flight path reconstruction is explained in Section III, and the methodology for aerodynamic model identification in Section IV. The results are presented in Section V, which contain results from the flight tests, flight path reconstruction, and the aerodynamic model identification. Finally, a brief flight mechanics analysis is presented in Section VI and conclusions are presented in Section VII.

II. Sub-Scale Model Description

The research vehicle used for the flight tests is a 4.6% sub-scale model of the Flying V (Fig. 2). It has been geometrically scaled as well as Froude scaled for the mass in order to maintain some similarity of flight conditions to the full-scale design [32]. The reference dimensions of the model are presented in Table 1. Figure 3 shows the wing planform, the mean aerodynamic chord, the center of gravity during the flight test campaign, and the moment reference centre. The model was primarily built from fibre glass sandwich material in order to achieve a lightweight structure while maintaining high stiffness to limit aerodynamic deflections in flight. This was done in order to ease comparisons of flight data to CFD and other analyses, since these analyses were performed on the jig shape of the aircraft, without taking aeroelastic deflections into account. Vacuum infusion in accurate moulds was used as the production technique. Furthermore, to ensure and validate accuracy, a portable coordinate measuring machine was used throughout production, enabling sub-millimeter tolerances and alignments. To reduce cost and complexity, mostly off the shelf components have been used. The vehicle is equipped with two 120 mm electric ducted fans, providing 80 N of static thrust each, powered by 12 cell LiPo batteries. Suitable commercial servos are used for actuating the control surfaces. The retractable landing gear is equipped with nose wheel steering and electromagnetically actuated brakes on the main wheels. Custom power redundancy circuitry was developed to power all aircraft systems in a redundant manner, reducing the possibility of incident due to power issues such as broken wires or battery depletion. Temperatures and current draw of critical system components is monitored live in order to further ensure flight safety. All air data, flight information and system health is sent to the ground station via two independent radio telemetry links, being displayed on custom ground displays for flight test engineers to monitor progress and assist the pilot. Lastly this information is also stored locally on the aircraft for redundant data storage.

On the outboard wing a transition strip was placed made out of carborundum particles with an average particle size of 180 μm. The strip was placed at 5% and 10% of the chord on the suction and pressure side, respectively. On the winglets, that also serve as vertical stabilizers, the same transition strip was applied at 10% of the chord.

Table 1 Reference geometry of the flight test article

Reference	Value
S	1.866 m^2
$\bar{c}$	0.817 m
b	3 m
$x_{\text{cg}}/\bar{c}$	34.02 %
$x_{\text{ref}}/\bar{c}$	25 %

A. Flight Test Instrumentation System

The model includes a Pixhawk 4 as the autopilot with a modified firmware to perform automated maneuvers for system identification. A Voyager GPS/INS μADC from Aeroprobe is the Digital Air Data Computer (DADC) used during the tests. A 5 hole pitot probe, also from Aeroprobe, is mounted on a boom extending forward of the nose of the model providing freestream airflow data. The combination of sensors present in the autopilot and the DADC provide measurements of the main variables of interest, such as airspeed,

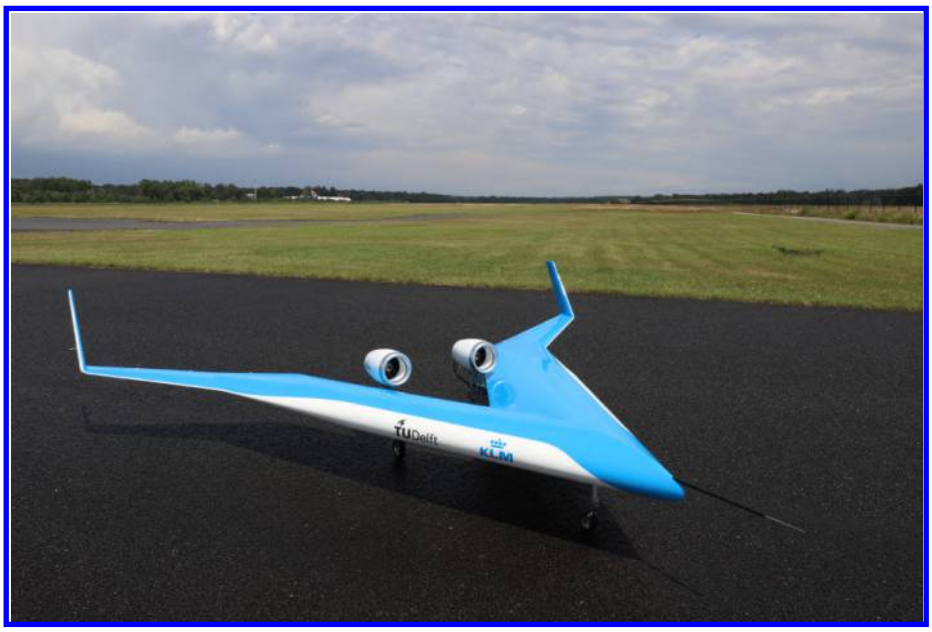

Fig. 2 4.6% sub-scale model used for the flight tests

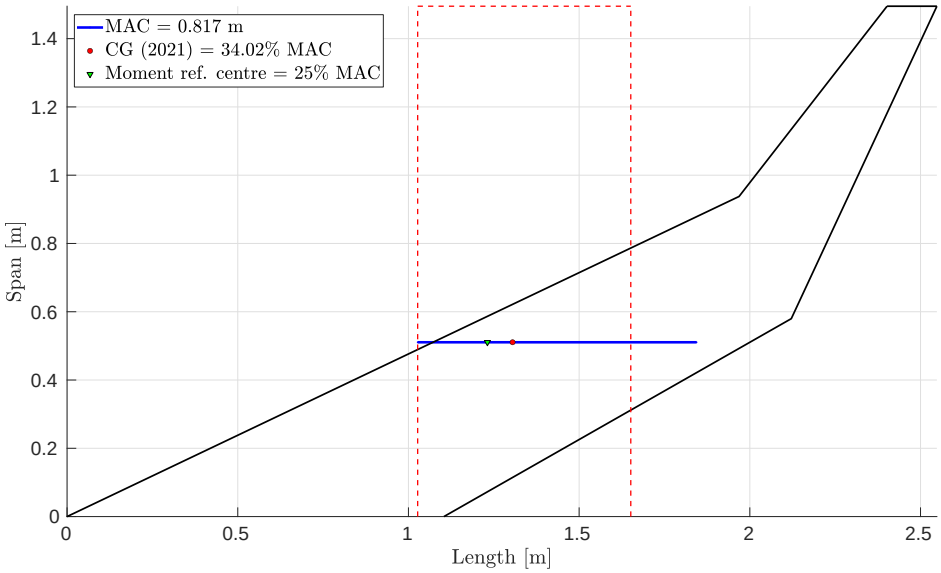

Fig. 3 Planform geometry of the flight test article indicating the mean-aerodynamic chord, the location of the center of gravity used for the flight tests, and the moment reference centre.

angle-of-attack, angle-of-sideslip, body accelerations, or angular rates. A summary of the available measured quantities and their characteristics is given in Table 2. The standard deviations of the accelerometers and gyros are taken from Ref. [33], the standard deviations of the true airspeed and flow angles are provided by the manufacturer, and the standard deviations of the GPS position, velocity and Euler angles are determined in calibration tests. The accurate location of the different systems was determined using a portable coordinate measurement machine alongside a 3D CAD model that was used during the design, manufacturing, and assembly. A schematic of the location of the most relevant systems is presented in Fig. 4

Table 2 Flight Test Instrumentation System description

Variable	Symbol	Units	Std. deviation	Sampling rate	Source
X_b-acceleration	A_x	m/s^2	$1.294 \cdot 10^{-2}$	50 Hz	MPU-6000 (Pixhawk 4)
Y_b-acceleration	A_y	m/s^2	$1.324 \cdot 10^{-2}$	50 Hz	MPU-6000 (Pixhawk 4)
Z_b-acceleration	A_z	m/s^2	$2.012 \cdot 10^{-2}$	50 Hz	MPU-6000 (Pixhawk 4)
X_b-angular rate	p	rad/s	$7.026 \cdot 10^{-4}$	50 Hz	MPU-6000 (Pixhawk 4)
Y_b-angular rate	q	rad/s	$6.325 \cdot 10^{-4}$	50 Hz	MPU-6000 (Pixhawk 4)
Z_b-angular rate	r	rad/s	$6.218 \cdot 10^{-4}$	50 Hz	MPU-6000 (Pixhawk 4)
True airspeed	V	m/s	0.25	100 Hz	Air data probe (DADC)
Angle-of-attack	α	deg	0.35	100 Hz	Air data probe (DADC)
Angle-of-sideslip	β	deg	0.35	100 Hz	Air data probe (DADC)
GPS position	$[x_E, y_E, z_E]$	m	[5, 5, 1]	100 Hz	Xsens MTi-G-710 (DADC)
GPS velocity	$[\dot{x}_E, \dot{y}_E, \dot{z}_E]$	m/s	[0.5, 0.5, 0.5]	100 Hz	Xsens MTi-G-710 (DADC)
Euler angles	$[\phi, \theta, \psi]$	deg	[0.3, 0.3, 1]	100 Hz	Xsens MTi-G-710 (DADC)

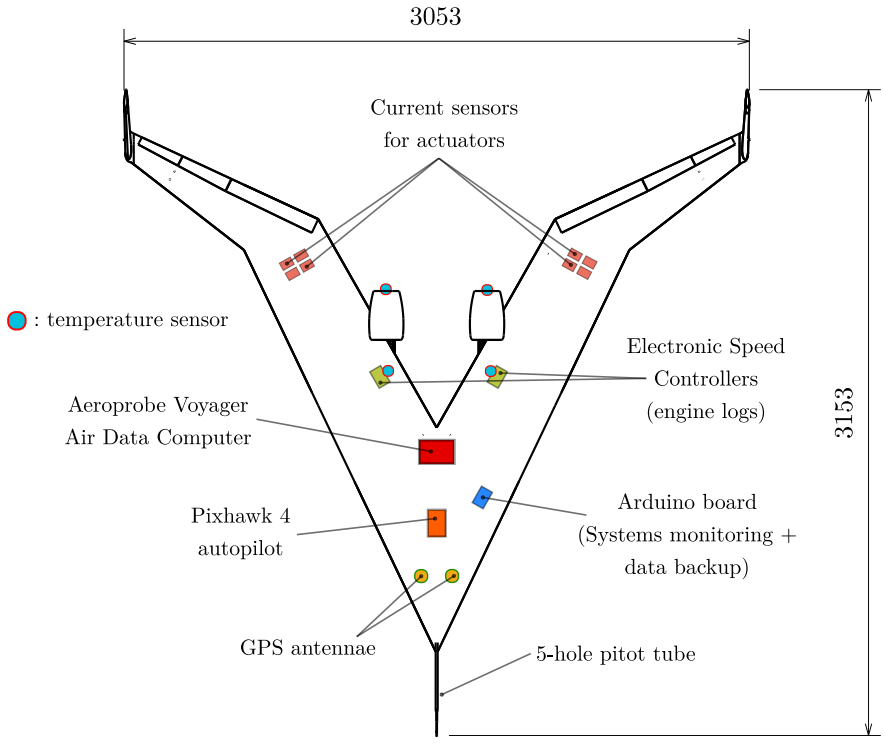

Fig. 4 Schematic of the locations of each measurement system, top view (dimensions in mm)

B. Mass model

The estimate of the inertia for the aircraft was done with a detailed 3D model created in CATIA, shown in Fig. 5. The model includes all components used in the construction of the aircraft including wiring, connectors, and fasteners. Each component was weighed before installing it into the aircraft and with these weights a uniform density was used in order to estimate the inertia contribution from each individual component. During large bonding/painting processes the masses of the components was recorded before and after, to calculate the amount of adhesives/paint that was added which was then distributed and included into the inertia estimation. Without access to an inertia swing to experimentally calculate the inertia it is hard to know how accurate the estimation is. However, the center of gravity estimated with the mass model is very close to the actual center of gravity of the aircraft, which serves as some validation of the estimation. The estimated values of the mass, center of gravity, and moments and products of inertia are presented in Table 3.

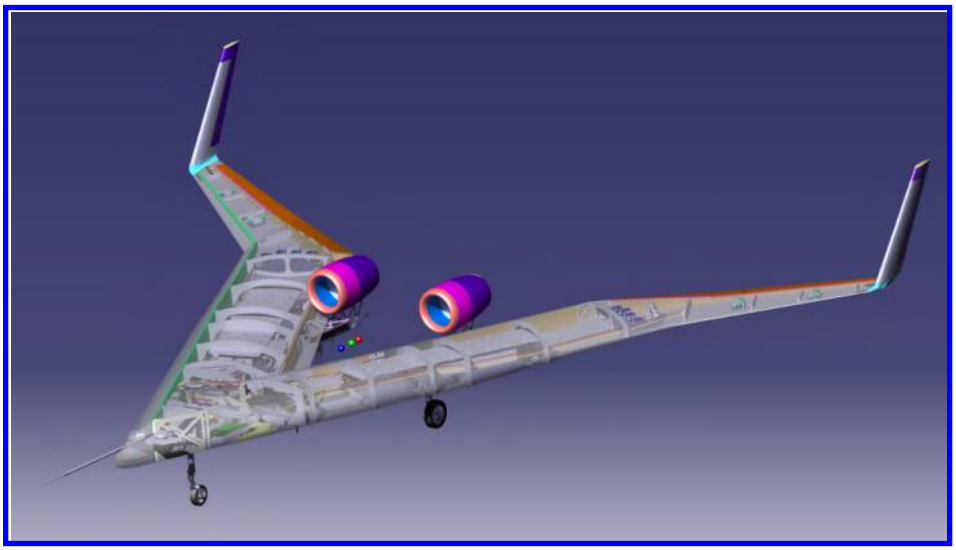

Fig. 5 CAD model of the research vehicle used for inertia estimation

Table 3 Mass and inertias of the sub-scale model

Reference	Value
mass	22.947 kg
$x_{cg}/\bar{c}$ (est.)	34.52 % MAC
I_{xx}	6.165 kg $\cdot$ m^2
I_{yy}	7.442 kg $\cdot$ m^2
I_{zz}	13.289 kg $\cdot$ m^2
I_{xy}	0.024 kg $\cdot$ m^2
I_{yz}	-0.002 kg $\cdot$ m^2
I_{xz}	0.397 kg $\cdot$ m^2

C. Control surfaces

The control surfaces are located on the trailing edge of the outboard section of the wing (elevons) and on the winglets (rudders). Three elevons are present on each side of the wing, acting like a single surface, and a rudder is present on each of the winglets. A control mixer was programmed to distribute the pitch and roll inputs to the left and right elevons, while the yaw input was mapped directly to the rudders. Differential aileron deflection was implemented to deflect the ailerons more up than down in order to minimize adverse

yaw effects.

Actuator dynamics are accounted for by using an *ARMAX* model for the servos identified in Ref. [34]. The model structure proposed in Ref. [35] was used, which is based on the internal wiring of the servo and its controller. The dynamic response of the servos was identified using the same kind of maneuvers perfomed during the flight tests (doublets and 3211-maneuvers) in a wind tunnel, achieving a validation relative RMS of 1.4% and a coefficient of determination of 99.88%.

$$A(z)y(t) = B(z)u(t - \tau_d) + C(z)v(t). \tag{1}$$

$$\begin{aligned} A(z) &= 1 - 1.402z^{-1} + 0.8776z^{-2} - 0.3216z^{-3} + 0.05933z^{-4} \\ B(z) &= 0.07146z^{-2} + 0.09506z^{-3} + 0.02848z^{-4} + 0.01754z^{-5} \\ C(z) &= 1 - 0.3946z^{-1} + 0.3627z^{-2} - 0.0497z^{-3} + 0.0144z^{-4} \end{aligned} \tag{2}$$

where y is the output, u is the input, v is the measurement error, z is the delay operator, and $\tau_d = 20$ ms is the dead time, a delay between the input and the start of the response.

III. Flight Path Reconstruction

The Two-Step Method (TSM), also known as *estimation-before-modeling* by some authors, is used to decouple the complex aerodynamic model identification problem into separate state estimation and parameter estimation problems [36]. It allows for a simplification of the analysis and to use linear regression techniques for the aerodynamic parameter estimation instead of solving the original output-error problem. A schematic of the method is shown in Fig. 6.

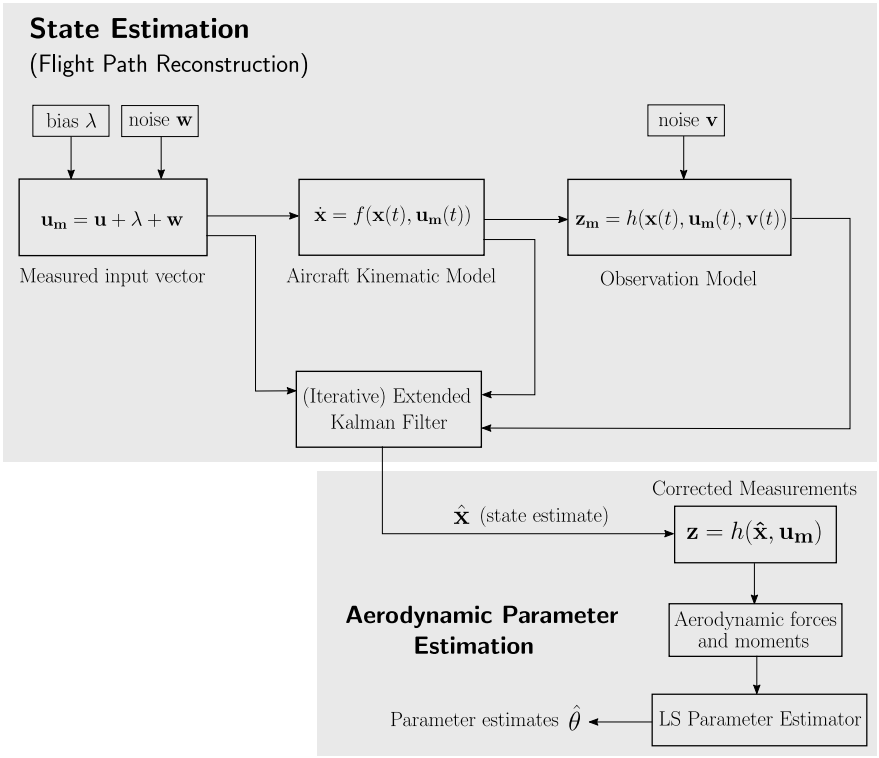

Fig. 6 Schematic of the Two-Step Method for system identification

At the core of the method there is an Iterated Extended Kalman Filter, whose task is to remove noise and biases from the measured states by taking into account the physical relations among inputs, observations,

and states. These relations are given by the aircraft equations of motion and an observation model which depends on the measured variables during the flight.

In this section, some of the blocks appearing in Fig. 6 are explained. First the model structure for the Kalman filter is presented in Subsection III.A. The aircraft kinematic model is represented by the state transition equations, which are stated in Subsection III.B. The observation model is presented in Subsection III.C, and finally a correction for the measured accelerations is explained in Subsection III.D.

A. Iterated Extended Kalman Filter

An aircraft is a dynamic system that can be represented in a general way by a nonlinear kinematic model $f(\bullet)$ and a nonlinear observation model $h(\bullet)$:

$$\begin{aligned} \dot{\mathbf{x}}(t) &= f(\mathbf{x}(t), \mathbf{u}(t), \mathbf{w}(t), t), \\ \dot{\mathbf{z}}(t) &= h(\mathbf{x}(t), \mathbf{u}(t), \mathbf{v}(t), t), \end{aligned} \tag{3}$$

where t is time, $\mathbf{x}$ is the state vector, $\mathbf{u}$ is the input vector, $\mathbf{w}$ is process noise, and $\mathbf{v}$ is measurement noise.

The classical Kalman filter is an optimal estimator for linear systems, but because of the nonlinearities present in the equations of motion it is not suitable for the task at hand. A solution based on the local linearization of the kinematic and observation models is the Extended Kalman Filter (EKF), which is however not optimal anymore. To alleviate this problem an Extended Kalman Filter with "local iterations" can be used, which minimizes the innacuracies arising from the linearization [37]. This method is known as an Iterated Extended Kalman Filter (IEKF). The details of the implementation of such a filter can be found in Ref. [36].

To decouple the flight path reconstruction and aerodynamic model identification problems, the input, state, and observation vectors must be defined in a specific way. In the Two-Step Method, the input vector to the IEKF consists of the measured accelerations and angular rates, which are in turn a combination of the true accelerations and angular rates $\mathbf{u}$, a bias term $\boldsymbol{\lambda}$, and white process noise $\mathbf{w}$. The rationale behind this definition is that the input vector to the Kalman Filter requires measurable parameters with known dependencies and whose derivatives do not appear in the kinematic equations [38]. Therefore,

$$\mathbf{u_m} = [A_{x\mathrm{m}}, A_{y\mathrm{m}}, A_{z\mathrm{m}}, p_\mathrm{m}, q_\mathrm{m}, r_\mathrm{m}]^T_{6\times 1} = \underbrace{\begin{bmatrix} A_x \\ A_y \\ A_z \\ p \\ q \\ r \end{bmatrix}}_{\mathbf{u}} + \underbrace{\begin{bmatrix} \lambda_x \\ \lambda_y \\ \lambda_z \\ \lambda_p \\ \lambda_q \\ \lambda_r \end{bmatrix}}_{\text{bias}} + \underbrace{\begin{bmatrix} w_x \\ w_y \\ w_z \\ w_p \\ w_q \\ w_r \end{bmatrix}}_{\text{noise}} \tag{4}$$

Accelerometer biases exist when the accelerometers are not located at the center of gravity, a situation that will always occur for the aircraft under study, since the center of gravity position is actually outside the outer mold line, behind the root airfoil trailing edge. Gyro biases occur when there are errors in the estimation of the aircraft moments and products of inertia [38]. These biases are estimated by augmenting the state vector of the Kalman Filter and adding the corresponding state transition equations. The observation vector is defined by the available measurements except the accelerations and angular rates:

$$\mathbf{z_m} = [x_{E\mathrm{m}}, y_{E\mathrm{m}}, z_{E\mathrm{m}}, \dot{x}_{E\mathrm{m}}, \dot{y}_{E\mathrm{m}}, \dot{z}_{E\mathrm{m}}, \phi_\mathrm{m}, \theta_\mathrm{m}, \psi_\mathrm{m}, V_\mathrm{m}, \alpha_\mathrm{m}, \beta_\mathrm{m}]^T_{12\times 1} \tag{5}$$

Finally, the state vector for the IEKF is defined by all the parameters that are required to construct the observation vector:

$$\mathbf{x} = [x_E, y_E, z_E, u, v, w, \phi, \theta, \psi]^T_{9\times 1} \tag{6}$$

The state vector is augmented with the unknown variables to be estimated in the process: biases from accelerometers and gyros, wind speed in North and East directions and the upwash coefficient at the probe

location. It is important to confirm that the system is still observable after adding the augmented states.

$$\mathbf{x_{aug}} = \begin{bmatrix} \mathbf{x} \\ \boldsymbol{\lambda} \\ W_{xE} \\ W_{yE} \\ C_{\alpha,up} \end{bmatrix}_{18\times 1} \tag{7}$$

B. Aircraft kinematic model

The aircraft kinematic model block from Fig. 6 is represented by the state transition equations in the IEKF. For an aircraft following a generic trajectory the nonlinear equations of motion should be used. These can be found in any flight mechanics textbook and are reproduced here for completeness. The evolution of the aircraft position in Earth-fixed NED reference frame is given by:

$$\begin{aligned} \dot{x}_E &= (u\cos\theta + (v\sin\phi + w\cos\phi)\sin\theta)\cos\psi - (v\cos\phi - w\sin\phi)\sin\psi + W_{xE}, \\ \dot{y}_E &= (u\cos\theta + (v\sin\phi + w\cos\phi)\sin\theta)\sin\psi + (v\cos\phi - w\sin\phi)\cos\psi + W_{yE}, \\ \dot{z}_E &= -u\sin\theta + (v\sin\phi + w\cos\phi)\cos\theta, \end{aligned} \tag{8}$$

The derivatives of the body velocities are written in terms of the measured accelerations and angular rates and the biases to be estimated:

$$\begin{aligned} \dot{u} &= (A_{x\mathrm{m}} - \lambda_x) - g\sin\theta + (r_\mathrm{m} - \lambda_r)v - (q_\mathrm{m} - \lambda_q)w, \\ \dot{v} &= (A_{y\mathrm{m}} - \lambda_y) + g\cos\theta\sin\phi + (p_\mathrm{m} - \lambda_p)w - (r_\mathrm{m} - \lambda_r)u, \\ \dot{w} &= (A_{z\mathrm{m}} - \lambda_z) + g\cos\theta\cos\phi + (q_\mathrm{m} - \lambda_q)u - (p_\mathrm{m} - \lambda_p)v, \end{aligned} \tag{9}$$

The derivatives of the Euler angles are:

$$\begin{aligned} \dot{\phi} &= (p_\mathrm{m} - \lambda_p) + ((q_\mathrm{m} - \lambda_q)\sin\phi + (r_\mathrm{m} - \lambda_r)\cos\phi)\tan\theta, \\ \dot{\theta} &= (q_\mathrm{m} - \lambda_q)\cos\phi - (r_\mathrm{m} - \lambda_r)\sin\phi, \\ \dot{\psi} &= ((q_\mathrm{m} - \lambda_q)\sin\phi + (r_\mathrm{m} - \lambda_r)\cos\phi)\frac{1}{\cos\theta}\,. \end{aligned} \tag{10}$$

Finally, additional transition equations are needed for the augmented states. The simplest approach is to consider they are time-invariant such that:

$$\dot{x}_k = 0, \tag{11}$$

which is a valid assumption and has offered good results with the Two-Step Method [20]. In this work the approach suggested in Ref. [36] is followed, which considers the augmented states as Markov processes:

$$\dot{x}_k = -\frac{1}{\tau_k}\cdot x_k + w_{x_k}. \tag{12}$$

In this expression τ_k is a correlation time and w_{x_k} artificial noise which is added to help the IEKF to converge. By combining Eqs. (8), (9), (10), and (12) into a nonlinear state transition model $f(\bullet)$, the state transition equations are written as:

$$\dot{\mathbf{x}} = f(\mathbf{x_{aug}}(t), \mathbf{u_m}(t), t) \tag{13}$$

C. Observation model

The observation equations relate the measured quantities to the inputs and the states. The aircraft position and velocity in Earth-fixed axes are given by the GPS module and are expressed in terms of the state and input vector as:

$$
\begin{aligned}
\dot{x}_{E\mathrm{m}} &= (u\cos\theta + (v\sin\phi + w\cos\phi)\sin\theta)\cos\psi - (v\cos\phi - w\sin\phi)\sin\psi + W_{xE} + v_{\dot{x}_E},\\
\dot{y}_{E\mathrm{m}} &= (u\cos\theta + (v\sin\phi + w\cos\phi)\sin\theta)\sin\psi + (v\cos\phi - w\sin\phi)\cos\psi + W_{yE} + v_{\dot{y}_E},\\
\dot{z}_{E\mathrm{m}} &= -u\sin\theta + (v\sin\phi + w\cos\phi)\cos\theta + v_{\dot{z}_E}.
\end{aligned} \tag{14}
$$

The expressions for the position in Earth-fixed axes and the aircraft Euler angles are simple since they are state variables:

$$
\begin{aligned}
x_{E\mathrm{m}} &= x_E + v_{xE},\\
y_{E\mathrm{m}} &= y_E + v_{yE},\\
z_{E\mathrm{m}} &= z_E + v_{zE}.
\end{aligned} \tag{15}
$$

$$
\begin{aligned}
\phi_{\mathrm{m}} &= \phi + v_\phi,\\
\theta_{\mathrm{m}} &= \theta + v_\theta,\\
\psi_{\mathrm{m}} &= \psi + v_\psi.
\end{aligned} \tag{16}
$$

Finally, the measured airspeed, angle-of-attack, and angle-of-sideslip are related to the state and input vector by the following expressions [12, 38]:

$$
\begin{aligned}
V_{\mathrm{m}} &= \sqrt{u^2 + v^2 + w^2} + v_{_V},\\
\alpha_{\mathrm{m}} &= (1 + C_{\alpha,up}) \cdot \mathrm{atan}\left(\frac{w}{u}\right) + \frac{(q_{\mathrm{m}} - \lambda_q) \cdot x_{probe}}{V} + v_\alpha,\\
\beta_{\mathrm{m}} &= \mathrm{atan}\left(\frac{v}{\sqrt{u^2 + w^2}}\right) - \frac{(r_{\mathrm{m}} - \lambda_r) \cdot x_{probe}}{V} + \frac{(p_{\mathrm{m}} - \lambda_p) \cdot z_{probe}}{V} + v_\beta.
\end{aligned} \tag{17}
$$

Note that the measured angle-of-attack is not the geometric angle-of-attack, but it includes the influence of an upwash coefficient $C_{\alpha,up}$ and a kinematically-induced angle due to the pitch rate and the position of the probe with respect to the center of gravity. The same is true for the sideslip angle. However, it was decided not to include the sidewash coefficient as it did not converge to a stable value and led to an overall worse convergence of the IEKF. Analogously to the state transition equations, Eqs. (14), (15), (16), and (17) can be combined in a nonlinear observation model $h(\bullet)$:

$$
\mathbf{z}_{\mathrm{m}} = h(\mathbf{x_{aug}}(t), \mathbf{u_m}(t), t) \tag{18}
$$

D. Correction for measured accelerations

In the previous sections, the respective locations of the measurement equipment relative to the center of gravity was not included in the expressions. However, the measured accelerations must be corrected for these offsets. A correction is derived in Ref. [12] and reproduced in Eq. (19). Applying this correction directly carries negative implications regarding the flight path reconstruction: 1) the variance for the acceleration measurements increase because of the error propagation in the calculation, and 2) the measured accelerations and angular rates contain a bias which is introduced into the linear accelerations. A better approach would be to apply this correction inside the IEKF, which would become much more complex as the linear accelerations become part of the state vector, and the angular rates derivatives need to be added as additional inputs [38]. Given that this is a preliminary study and the small number of flights performed to date, it was decided to apply the correction directly to the measured accelerations and and confirm its validity when more flight data is available.

$$
\begin{aligned}
A_{x,\mathrm{cg}} &= A_{x,\mathrm{acc}} + (x_{\mathrm{cg}} - x_{\mathrm{acc}}) \cdot (q^2 + r^2) - (y_{\mathrm{cg}} - y_{\mathrm{acc}}) \cdot (pq - \dot{r}) - (z_{\mathrm{cg}} - z_{\mathrm{acc}}) \cdot (pr + \dot{q}),\\
A_{y,\mathrm{cg}} &= A_{y,\mathrm{acc}} + (y_{\mathrm{cg}} - y_{\mathrm{acc}}) \cdot (r^2 + p^2) - (z_{\mathrm{cg}} - z_{\mathrm{acc}}) \cdot (qr - \dot{p}) - (x_{\mathrm{cg}} - x_{\mathrm{acc}}) \cdot (qp + \dot{r}),\\
A_{z,\mathrm{cg}} &= A_{z,\mathrm{acc}} + (z_{\mathrm{cg}} - z_{\mathrm{acc}}) \cdot (p^2 + q^2) - (x_{\mathrm{cg}} - x_{\mathrm{acc}}) \cdot (rp - \dot{q}) - (y_{\mathrm{cg}} - y_{\mathrm{acc}}) \cdot (rq + \dot{p}).
\end{aligned} \tag{19}
$$

IV. Aerodynamic Model Identification

The second step of the TSM is the aerodynamic parameter estimation. The flight path reconstruction provides clean estimates of the states, which form the independent variables that will be used to model the aerodynamic coefficients. Noise is then ideally only present in the accelerations and angular rates, used to calculate the dependent variable (each aerodynamic coefficient). This allows the use of classical regression techniques. The methodology for the aerodynamic identification is discussed in this section; first the aerodynamic coefficients to estimate are defined, and a polynomial model is postulated based on previous wind-tunnel tests followed by the explanation of the parameter estimation process. Ordinary Least Squares are used for the regression and the model structure is determined using a stepwise regression technique. The model validation is done by means of an independent validation dataset not used for the identification, and to avoid collinearity problems, the selected regressors are orthogonalized. A thrust model for the engine is derived with which the engine contributions to the forces and moments are subtracted before the identification, and finally the test point selection is briefly discussed.

A. Definition of aerodynamic coefficients

The aerodynamic force coefficients along the X, Y, Z directions are the dependent variables to be estimated. The direct engine contribution is subtracted so that the results do not depend on the engine used. Therefore, these coefficients refer to the airframe forces and moments only and are defined as:

$$
\begin{aligned}
C_X(\chi) &= \frac{X(\chi)}{qS} = \frac{mA_x - X_{\mathrm{e}}}{qS} = \frac{m}{qS}(\dot{u} + qw - rv + g\sin\theta) - \frac{X_{\mathrm{e}}}{qS},\\
C_Y(\chi) &= \frac{Y(\chi)}{qS} = \frac{mA_y - Y_{\mathrm{e}}}{qS} = \frac{m}{qS}(\dot{v} + ru - pw - g\cos\theta\sin\phi) - \frac{Y_{\mathrm{e}}}{qS},\\
C_Z(\chi) &= \frac{Z(\chi)}{qS} = \frac{mA_z - Z_{\mathrm{e}}}{qS} = \frac{m}{qS}(\dot{w} + pv - qu - g\cos\theta\cos\phi) - \frac{Z_{\mathrm{e}}}{qS}.
\end{aligned} \tag{20}
$$

with the state vector χ defined by the airspeed, the angles of attack and sideslip, the dimensionless angular rates, and the control surface deflections:

$$
\chi = [V, \alpha, \beta, \hat{p}, \hat{q}, \hat{r}, \delta_e, \delta_a, \delta_r] \in \mathbb{R}^9 \tag{21}
$$

The angular rates are made dimensionless with the MAC and the wingspan:

$$
\hat{p} = \frac{pb}{2V}, \quad \hat{q} = \frac{q\bar{c}}{2V}, \quad \hat{r} = \frac{rb}{2V}. \tag{22}
$$

The deflections for the different control groups are defined as follows:

$$
\begin{aligned}
&\delta_e > 0 \rightarrow \text{ elevator down},\\
&\delta_a = \frac{\delta_{a,L} + \delta_{a,R}}{2}, \quad \delta_{a,L} > 0 \rightarrow \text{ left aileron down }, \delta_{a,R} > 0 \rightarrow \text{ right aileron up},\\
&\delta_r = \delta_{r,L} = \delta_{r,R} > 0 \rightarrow \text{ rudder right}.
\end{aligned} \tag{23}
$$

The moment coefficients are defined following the formulation from Ref. [39], again subtracting the engine

contribution:

$$
\begin{aligned}
C_l(\chi) &= \frac{L(\chi)}{qSb} = \frac{1}{qSb}\left(I_x\dot{p} - (I_y - I_z)qr - I_{xz}(\dot{r} + pq) - L_\mathrm{e}\right), \\
C_m(\chi) &= \frac{M(\chi)}{qS\bar{c}} = \frac{1}{qS\bar{c}}\left(I_y\dot{q} - (I_z - I_x)qr - I_{xz}(r^2 - p^2) + M_\mathrm{gyroscopic} - M_\mathrm{e}\right), \\
C_n(\chi) &= \frac{N(\chi)}{qSb} = \frac{1}{qSb}\left(I_z\dot{r} - (I_x - I_y)pq - I_{xz}(\dot{p} - qr) - N_\mathrm{e}\right).
\end{aligned} \tag{24}
$$

From Eqs. (24) it can be seen that the derivatives of the angular rates $\dot{p}, \dot{q}, \dot{r}$ are needed to calculate the aerodynamic moment coefficients. These variables however are not filtered by the IEKF and contain measurement errors, which makes the numerical differentiation problematic as it will amplify the present noise. Here the approach presented in Ref. [40] is followed: the measured angular rates are fitted every 5 points using second-order polynomials, the fitted polynomials are differentiated and the result is filtered using a smoother filter.

B. Model postulation

In Ref. [8] polynomial and spline models were identified using wind tunnel data from a half model of the Flying V, manufactured using the same moulds and techniques as the flight vehicle studied here. Based on the flight envelope during the flight tests, it can be reasoned that a polynomial model will suffice for the aerodynamic identification using the data gathered to date. If excursions to the edges of the flight envelope are done in the future, a spline model would be a better choice. Each aerodynamic coefficient can be written as:

$$
\mathbf{y} = \theta_0 + \sum_{j=1}^{n} \theta_j \mathbf{p}_j, \tag{25}
$$

or:

$$
\mathbf{y} = X \cdot \boldsymbol{\theta}; \qquad X = [1, \mathbf{p}_1, \mathbf{p}_2, ..., \mathbf{p}_n], \tag{26}
$$

where $\mathbf{p}_j$ are functions of the independent variables (regressors), X is the regression matrix, and $\boldsymbol{\theta}$ is the parameter vector to be estimated.

C. Ordinary Least Squares

Ordinary Least Squares (OLS) is the simplest form of least-squares regression and the method of choice for the present work, since the noise probability density is unknown. It is assumed that 1) the independent variables are not contaminated with noise, 2) the dependent variable is contaminated with uniformly distributed noise (white noise), and 3) the residuals are uncorrelated with the independent variables. If these assumptions hold, the Gauss-Markov Theorem states that the OLS estimator is the Best Linear Unbiased Estimator (BLUE) [41], where "best" implies minimum variance, and it can also be shown that the estimates are consistent and efficient [42]. On the other hand, if these assumptions are not true, the estimates could be inaccurate, so they need to be tested to guarantee that OLS is indeed a valid estimation method. If errors are present in the independent variables the estimates will be biased and the covariance of the estimates will be affected [43], which highlights the need for the state estimation.

The aerodynamic force and moment coefficients are the dependent variables to estimate, which are asummed to be contaminated with white noise:

$$
\mathbf{y_m}(i) = \mathbf{y}(i) + \mathbf{r}(i), \qquad i = 1, 2, ..., N \tag{27}
$$

where $\mathbf{y_m}$ is the measurement vector, $\mathbf{y}$ is the true value of the dependent variable, and $\mathbf{r}$ is a vector of measurement errors or residuals. These three vectors have dimensions of $[N \times 1]$, where N is the number of samples.

The residuals are assumed to be zero-mean and to have a constant covariance:

$$\mathrm{E}[\mathbf{r}] = 0, \quad \mathrm{E}[\mathbf{r}\mathbf{r}^T] = \sigma^2 I. \tag{28}$$

These assumptions lead to a simple expression for the cost function J_{OLS} and the parameter vector to minimize it ($\hat{\boldsymbol{\theta}}$):

$$J_{\mathrm{OLS}} = \frac{1}{2}[\mathbf{y_m} - X\boldsymbol{\theta}]^T[\mathbf{y_m} - X\boldsymbol{\theta}] = \frac{1}{2}[\mathbf{r}^T\mathbf{r}], \qquad \hat{\boldsymbol{\theta}} = (X^TX)^{-1}X^T\mathbf{y_m} \tag{29}$$

In order to derive confidence bounds for the parameters and the model output the noise is assumed to be given by a normal distribution, an assumption which is checked afterwards. The measurement error variance σ^2 is unknown and needs to be estimated from the measured data. An unbiased but model-dependent estimate for σ^2 can be found based on the residuals:

$$\hat{\sigma}^2 = \frac{\sum_{i=1}^{N}[z(i) - \hat{\mathbf{y}}(i)]^2}{N - n}, \tag{30}$$

which only gives adequate results if the model structure is adequate [43].

As pointed out in Refs. [44, 45], the assumption of white residuals is an unrealistic one in flight test data as the samples are usually correlated in time. In these situations it is still possible to apply OLS and use a corrected expression to calculate the parameter covariances, which takes into account the residual's correlation by considering the residual as a zero mean, weakly stationary random process [44]:

$$\mathrm{Cov}\left(\hat{\boldsymbol{\theta}}\right) = (X^TX)^{-1}\left(\sum_{i=1}^{N}\chi(i)\sum_{j=1}^{N}\hat{\mathcal{R}}_{vv}(i-j)\chi^T(j)\right)(X^TX)^{-1}, \tag{31}$$

where χ^T is the ith row of the regression matrix X and $\hat{\mathcal{R}}_{vv}(i-j)$ is estimated by:

$$\hat{\mathcal{R}}_{vv}(k) = \frac{1}{N}\sum_{i=1}^{N-k} v(i)v(i+k); \quad k = 0, 1, 2, ..., r. \tag{32}$$

Since the correlation is only strong for samples that are close together in time, a small value of r is usually sufficient for a good estimate of the autocorrelation.

D. Model selection

To determine a suitable model structure for each aerodynamic coefficient, the procedure for model selection presented in Ref. [8] is used. Some additional ideas incorporated from the work of Ulbrich [26, 27] are included here: the standard deviation of the PRESS statistic is adopted as an additional metric for model selection, the formulation to calculate the PRESS statistic is used, and model hierarchy is enforced.

To ensure a parsimonious model and avoid over-parameterization, the partial F-statistic must be higher than a certain threshold for a certain regressor to be considered significant and enter the model. A value of $F_p = 12$ to enter the model is used as suggested by Montgomery [43].

Models with high SVD condition indices are discarded to avoid numerical inaccuracies due to near-linear dependencies (collinearity) among the regressors [46]. According to Ref. [13], a condition index of about 35 would suggest moderate collinearity among the regressors in the model, and a condition index of 100 would suggest severe collinearity problems.

E. Model validation

The estimated aerodynamic model is validated using a third of the gathered flight data, which conforms the so-called validation dataset. This is done in order to avoid over-parameterization, since the model fit from the estimation dataset always improves with the addition of new regressors to the model. The Root Mean Square Error (RMS) of the residuals from both the estimation and the validation datasets is used to assess

the overall model fit. Indicators of a good model are not only small values of the relative RMS, but also that the RMS from the estimation and validation datasets have similar values.

In addition, an independent validation dataset allows for a way to discard insignificant regressors on top of the statistical correlations mentioned above. As regressors are added to the model the estimation RMS keeps decrecreasing in a monotonic way, and for a certain number of regressors the validation RMS follows the same trend. There is a point, however, where new regressors start to model features that are only present in the estimation dataset. At this point, the validation RMS starts to increase as the measurement noise is not the same in both datasets. Thus, the evolution of the RMS of the estimation and validation residuals, with the addition of regressors to the model, can offer useful information in order to validate a certain model structure.

Finally, some common statistical metrics such as the F-statistic or the coefficient of determination are examined before validating a model, and the normality of the residuals is assessed, as it is the main assumption required to derive confidence bounds.

F. Regressors orthogonalization

After the non-orthogonal models are calculated, an orthogonal pool of regressors is generated with the regressors in the model, using the methodology proposed by Morelli and Deloach [47]. The regressors are orthogonalized from most significant to least significant, which is determined by the order of entrance in the stepwise regression routine. This procedure was followed in Ref. [8] to identify an aerodynamic model of the Flying V from wind tunnel data and led to models with tight confidence bounds and good prediction capabilities while removing all issues which arise from collinearity.

Starting from the bias term ($\mathbf{p}_0 = \boldsymbol{\xi}_0 = \mathbf{1}$), all regressors are successively orthogonalized with respect to the previous ones. The j^{th} orthogonal function is given by:

$$\boldsymbol{\xi}_j = \mathbf{p}_j - \sum_{k=0}^{j-1} \gamma_{kj} \boldsymbol{\xi}_k; \quad \gamma_{kj} = \frac{\boldsymbol{\xi}_k^T \mathbf{p}_j}{\boldsymbol{\xi}_k^T \boldsymbol{\xi}_k}, \qquad j = 1, 2, ..., n \tag{33}$$

By rearranging the indices γ_{kj} in a matrix G, one can express the orthogonal regressors (columns of Ξ) in terms of the original regressors (columns of X) as:

$$\Xi = X \cdot G^{-1}; \qquad \Xi = [\boldsymbol{\xi}_0, \boldsymbol{\xi}_1, ..., \boldsymbol{\xi}_n], \quad X = [\mathbf{p}_0, \mathbf{p}_1, ..., \mathbf{p}_n] \tag{34}$$

G. Engine model

The forces and moments from Eqs. (20) and (24) include the contribution of the propulsion system, two electric ducted fans mounted on top of the wing. The contribution of the engines to the forces and moments is quantified by using a model for the thrust coefficient, identified from the wind tunnel data of Ref. [9] using Ordinary Least Squares. The result is subtracted from the estimated forces and moments before the parameter estimation. The model depends on the advance ratio, defined as $J = V/(n_\text{e} D_\text{e})$, where n_e is the rotational speed of the fan, D_e is its diameter, and V the airspeed:

$$C_T = -0.721 \cdot J + 0.954; \tag{35}$$

The thrust for a single engine directly follows as:

$$T = \rho n_\text{e}^2 D_\text{e}^4 C_T, \tag{36}$$

This linear model is only valid over a limited range of advance ratios, since at low advance ratios there is flow separation on the fan blades. Since the engines' location was accurately known, it was decided to estimate the engine contribution to the aircraft forces and moments using this thrust model. The airspeed during the flight tests ranged between approximately 30 and 40 m/s, while the engine model was constructed at 15-20 m/s. The effect of Reynolds number on the thrust curve is therefore not included herein [48]. Attempts of including engine variables as additional regressors in the aerodynamic identification led to poor quality models so this approach was discarded in favor of the extrapolation of the existing engine model.

H. Test point selection

To generate data with relevant information content for the aerodynamic identification, the on-board autopilot is programmed to execute 3211-maneuvers (also known as Koehler inputs) and doublets in a repeatable and consistent way. The maneuvers can be tuned by changing the duration and the magnitude in order to better excite the aircraft eigenmotions. These maneuvers are deemed more practical and safer to test than long frequency sweeps, and are commonly used for aircraft system identification purposes [19, 21, 38]. Only one control group (elevators, ailerons, or rudders) is actuated for each maneuver and the other two groups are kept constant and equal to their trimmed values at the beginning of the maneuver. The dataset is completed with manually flown maneuvers by the pilot and with data at different flight conditions (cruise, turns, climb, and descent).

V. Results

In this section the outcomes of the previously mentioned methodology are discussed. The results of the flight tests are presented in subsection V.A. Then the flight path reconstruction results are shown for both longitudinal and lateral maneuvers in subsection V.B and the estimated states, biases, and upwash coefficient are discussed. The results from the aerodynamic model identification are presented in subsection V.C, followed by the comparison of the results to with previous wind-tunnel tests in subsection V.D.

A. Flight test results

The commanded deflections and the raw measurements of the accelerations and angular rates during two representative maneuvers are presented in Fig. 7 and Fig. 8. The executed longitudinal maneuver (Fig. 7) generates a strong response in the vertical acceleration and the pitch rate as expected, with a smaller effect on the forward acceleration. The yaw rate remains more or less unaffected, whereas the roll rate presents oscillations due to a lightly damped Dutch roll mode which was observed during the flights. This effect is more clear for the lateral maneuver in Fig. 8, where a 3211-input from the rudders generates a strong oscillatory response on the roll rate and smaller but still noticeable oscillatory responses on the yaw rate and the pitch rate. The lateral force and the vertical force are slightly affected by the rudder input, but otherwise they remain fairly constant.

In Fig. 9 the data points assigned to the estimation and validation datasets are represented along with the convex hull of the estimation dataset, which determines the region of validity of the model. Outside of the convex hull no measurements are available, so using the estimated model would imply an extrapolation of the results. It can be seen how the majority of the validation data falls inside the convex hull, so the estimated aerodynamic model is considered valid for all the validation data.

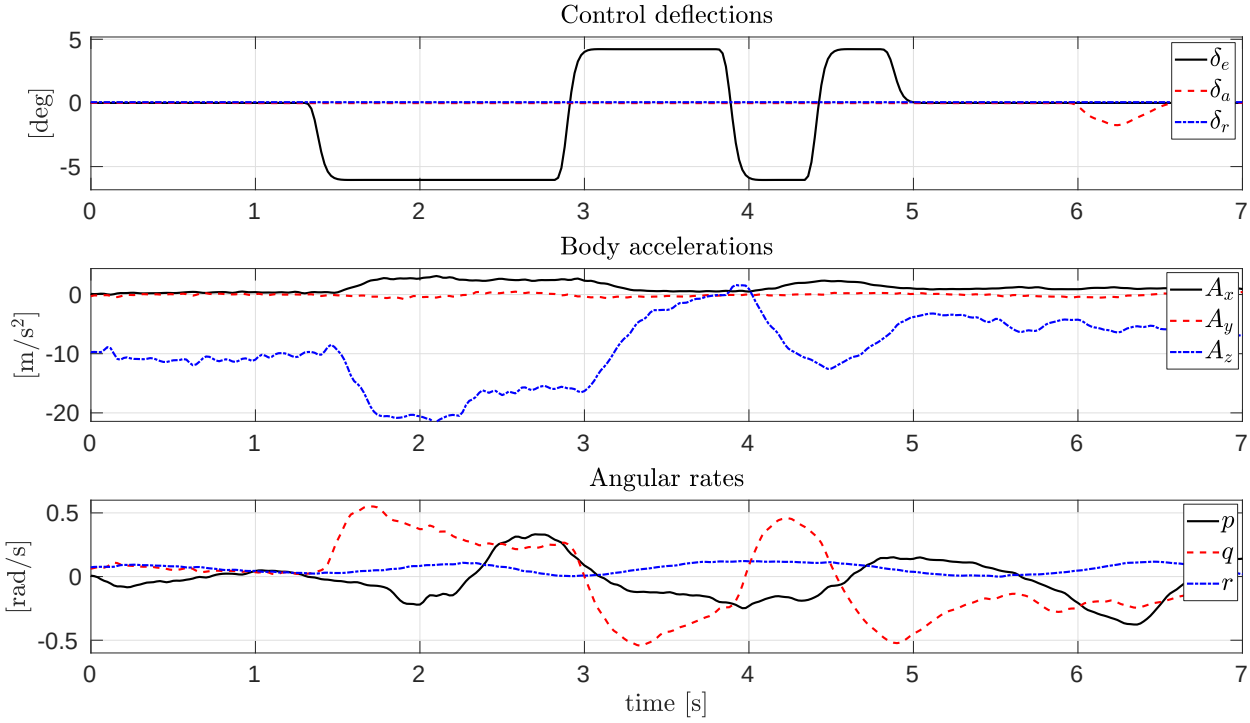

Fig. 7 Commanded control surface deflections and measured accelerations and angular rates during the execution of a longitudinal maneuver (3211-maneuver on the elevator)

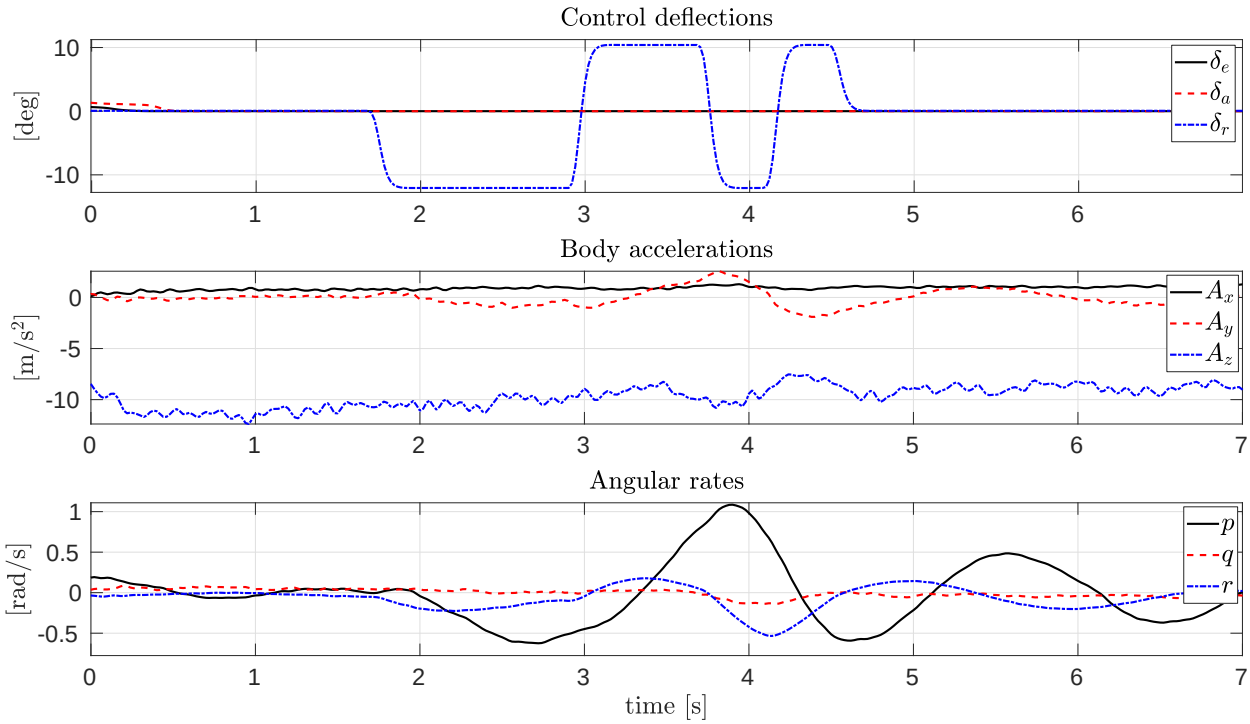

Fig. 8 Commanded control surface deflections and measured accelerations and angular rates during the execution of a lateral maneuver (3211-maneuver on the rudder)

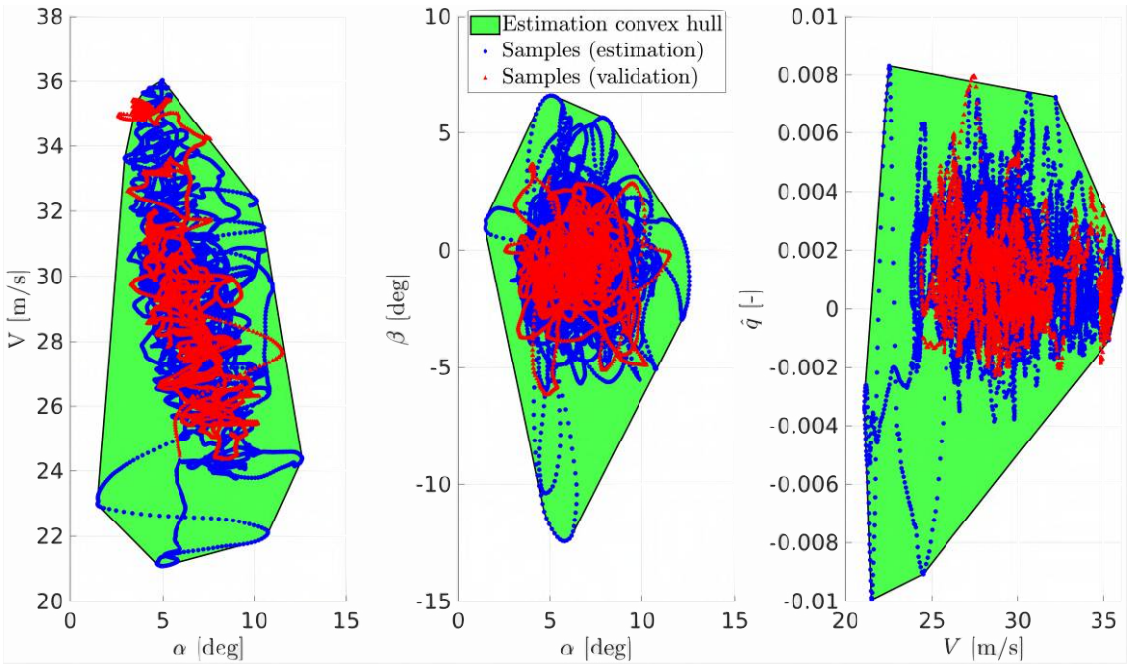

Fig. 9 $\alpha - V$, $\alpha - \beta$, and $V - \hat{q}$ cuts of the convex hull of the estimation dataset, which determines the region of validity of the identified aerodynamic model

B. Flight path reconstruction

The flight path reconstruction results are presented here for the two maneuvers mentioned above as representative examples. The estimated states for a 3211-input on the elevator are shown in Fig. 10, and for a 3211-input on the rudders in Fig. 11. The estimated sensor biases and upwash coefficient are averaged over all flights and presented in Table. 4 along with their associated standard deviation.

Table 4 Average estimated values of the augmented states (upwash coefficient and sensor biases)

	$C_{\alpha,up}$	λ_x	λ_y	λ_z	λ_p	λ_q	λ_r
Avg. value	$1.89 \cdot 10^{-1}$	$1.59 \cdot 10^{-1}$	$4.69 \cdot 10^{-2}$	$-2.31 \cdot 10^{-1}$	$-7.10 \cdot 10^{-3}$	$-2.90 \cdot 10^{-3}$	$-9.68 \cdot 10^{-4}$
Std. dev.	$6.40 \cdot 10^{-2}$	$1.70 \cdot 10^{-2}$	$4.47 \cdot 10^{-2}$	$3.34 \cdot 10^{-2}$	$5.53 \cdot 10^{-4}$	$4.74 \cdot 10^{-4}$	$4.77 \cdot 10^{-4}$

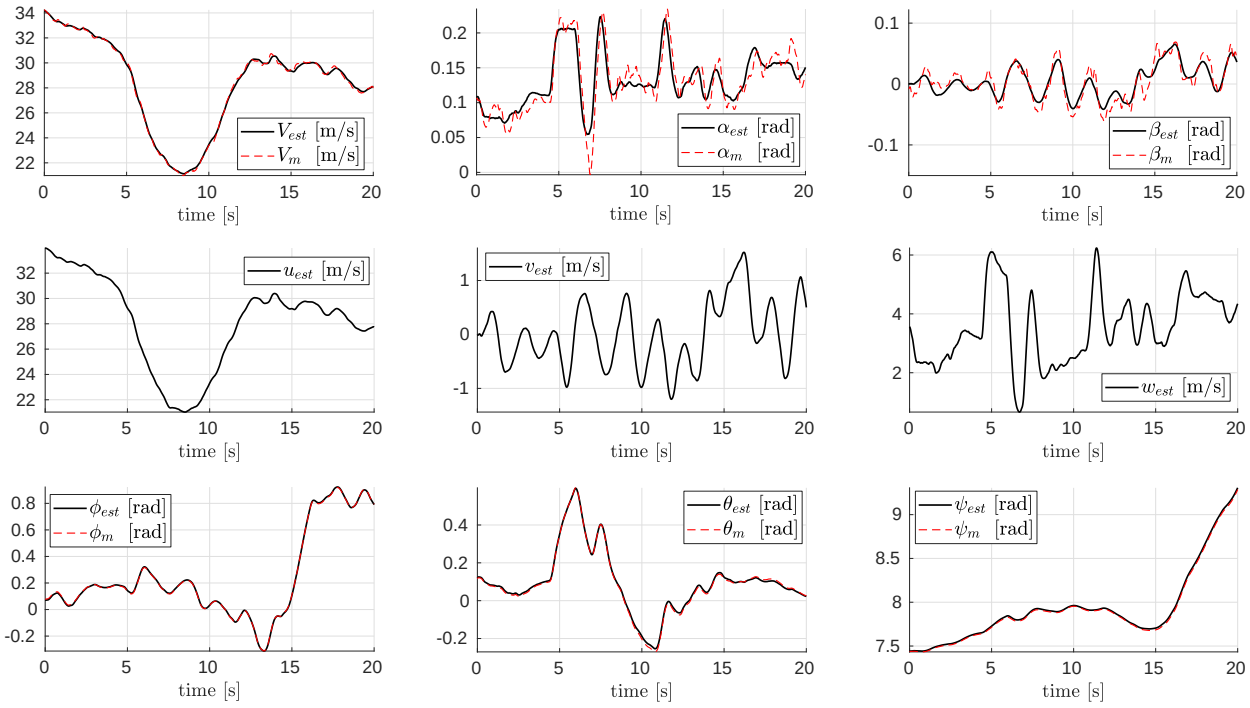

Fig. 10 Measured and estimated states during a programmed 3211-maneuver on the elevator: airspeed, flow angles, body velocities, and Euler angles

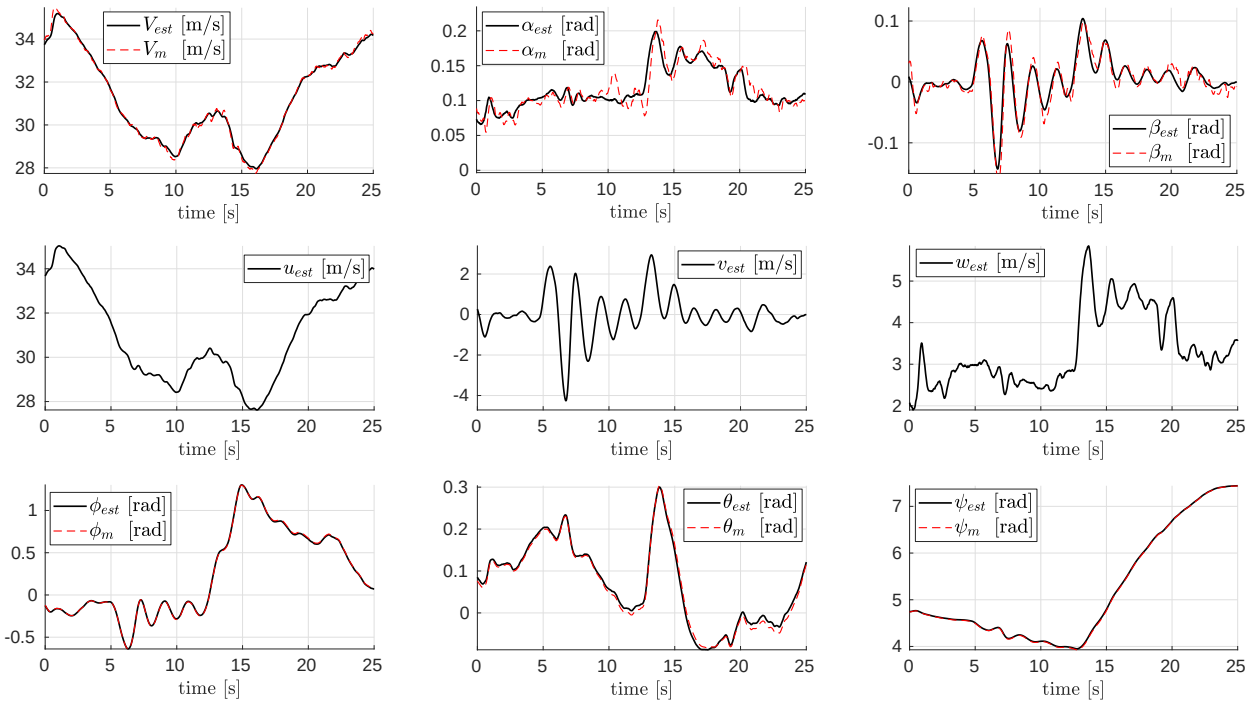

Fig. 11 Measured and estimated states during a programmed 3211-maneuver on the rudders

C. Aerodynamic model identification

The identified aerodynamic model structure is shown in Eq. (37). The estimated values for the coefficients are given in Table 5, and fit statistics for the models are presented in Table 6.

As a remark, no assumptions are made to separate longitudinal and lateral-directional coefficients, but since no significant cross-couplings are found during the regression the longitudinal and lateral-directional coefficients become effectively decoupled.

$$
\begin{aligned}
C_X &= C_{X0} + C_{X\alpha} \cdot \alpha + C_{X\alpha^2} \cdot \alpha^2 + C_{X\delta_e} \cdot \delta_e \\
C_Y &= C_{Y0} + C_{Y\beta} \cdot \beta + C_{Y\hat{r}} \cdot \hat{r} + C_{Y\delta_a} \cdot \delta_a + C_{Y\delta_r} \cdot \delta_r \\
C_Z &= C_{Z0} + C_{Z\alpha} \cdot \alpha + C_{Z\hat{q}} \cdot \hat{q} + C_{Z\delta_e} \cdot \delta_e \\
C_l &= C_{l0} \ + C_{l\beta} \cdot \beta + C_{l\hat{p}} \cdot \hat{p} + C_{l\hat{r}} \cdot \hat{r} + C_{l\delta_a} \cdot \delta_a + C_{l\delta_r} \cdot \delta_r \\
C_m &= C_{m0} + C_{m\alpha} \cdot \alpha + C_{m\hat{q}} \cdot \hat{q} + C_{m\delta_e} \cdot \delta_e \\
C_n &= C_{n0} + C_{n\beta} \cdot \beta + C_{n\hat{p}} \cdot \hat{p} + C_{n\hat{r}} \cdot \hat{r} + C_{n\delta_a} \cdot \delta_a + C_{n\delta_r} \cdot \delta_r
\end{aligned}
\tag{37}
$$

Table 5 Estimated values of the aerodynamic coefficients

	Parameter	Value	Std. error		Parameter	Value	Std.error
C_X	C_{X0}	$-3.617 \cdot 10^{-2}$	$4.794 \cdot 10^{-3}$	C_l	C_{l0}	$-1.510 \cdot 10^{-3}$	$1.146 \cdot 10^{-4}$
	$C_{X\alpha}$	$8.193 \cdot 10^{-2}$	$8.227 \cdot 10^{-2}$		$C_{l\beta}$	$-1.084 \cdot 10^{-1}$	$4.022 \cdot 10^{-3}$
	$C_{X\alpha^2}$	1.796	$3.408 \cdot 10^{-1}$		$C_{l\hat{p}}$	$-2.004 \cdot 10^{-1}$	$9.864 \cdot 10^{-3}$
	$C_{X\delta_e}$	$3.230 \cdot 10^{-2}$	$1.595 \cdot 10^{-2}$		$C_{l\hat{r}}$	$1.396 \cdot 10^{-1}$	$1.317 \cdot 10^{-2}$
					$C_{l\delta_a}$	$1.134 \cdot 10^{-1}$	$4.58 \cdot 10^{-3}$
					$C_{l\delta_r}$	$-1.003 \cdot 10^{-2}$	$2.736 \cdot 10^{-3}$
C_Y	C_{Y0}	$-4.466 \cdot 10^{-3}$	$2.010 \cdot 10^{-3}$	C_m	C_{m0}	$2.654 \cdot 10^{-2}$	$2.005 \cdot 10^{-3}$
	$C_{Y\beta}$	$-4.378 \cdot 10^{-1}$	$6.530 \cdot 10^{-3}$		$C_{m\alpha}$	$-2.641 \cdot 10^{-1}$	$2.026 \cdot 10^{-2}$
	$C_{Y\hat{r}}$	$3.328 \cdot 10^{-1}$	$4.843 \cdot 10^{-3}$		$C_{m\hat{q}}$	-1.193	$2.794 \cdot 10^{-1}$
	$C_{Y\delta_a}$	$8.912 \cdot 10^{-2}$	$6.640 \cdot 10^{-3}$		$C_{m\delta_e}$	$-2.790 \cdot 10^{-1}$	$1.802 \cdot 10^{-2}$
	$C_{Y\delta_r}$	$-8.839 \cdot 10^{-2}$	$1.719 \cdot 10^{-3}$				
C_Z	C_{Z0}	$2.749 \cdot 10^{-2}$	$1.031 \cdot 10^{-2}$	C_n	C_{n0}	$4.016 \cdot 10^{-4}$	$4.170 \cdot 10^{-5}$
	$C_{Z\alpha}$	-2.786	$1.055 \cdot 10^{-1}$		$C_{n\beta}$	$5.511 \cdot 10^{-2}$	$1.680 \cdot 10^{-3}$
	$C_{Z\hat{q}}$	-4.147	1.394		$C_{n\hat{p}}$	$-1.566 \cdot 10^{-2}$	$4.737 \cdot 10^{-3}$
	$C_{Z\delta_e}$	$-5.706 \cdot 10^{-1}$	$8.488 \cdot 10^{-2}$		$C_{n\hat{r}}$	$-7.683 \cdot 10^{-2}$	$2.571 \cdot 10^{-3}$
					$C_{n\delta_a}$	$-6.664 \cdot 10^{-3}$	$4.324 \cdot 10^{-3}$
					$C_{n\delta_r}$	$2.036 \cdot 10^{-2}$	$8.821 \cdot 10^{-4}$

Table 6 Fit statistics for the identified models

	RMS_{rel} (est.)	RMS_{rel} (val.)	$\max(\lvert\mathbf{v}_{\text{est}}\rvert)$	$\max(\lvert\mathbf{v}_{\text{val}}\rvert)$
C_X	5.51%	6.76%	27.50%	38.55%
C_Y	3.25%	6.41%	25.99%	34.11%
C_Z	4.46%	5.25%	27.50%	26.06%
C_l	7.06%	8.27%	38.41%	51.43%
C_m	6.99%	9.96%	45.82%	44.80%
C_n	3.08%	5.56%	20.56%	24.21%

A comparison between the measured aerodynamic coefficients and those estimated by the model is shown in

Fig. 12 for two of the maneuvers flown during the tests. It must be noted that the coefficients displayed in the figure include the engine contribution to compare to the raw measurements.

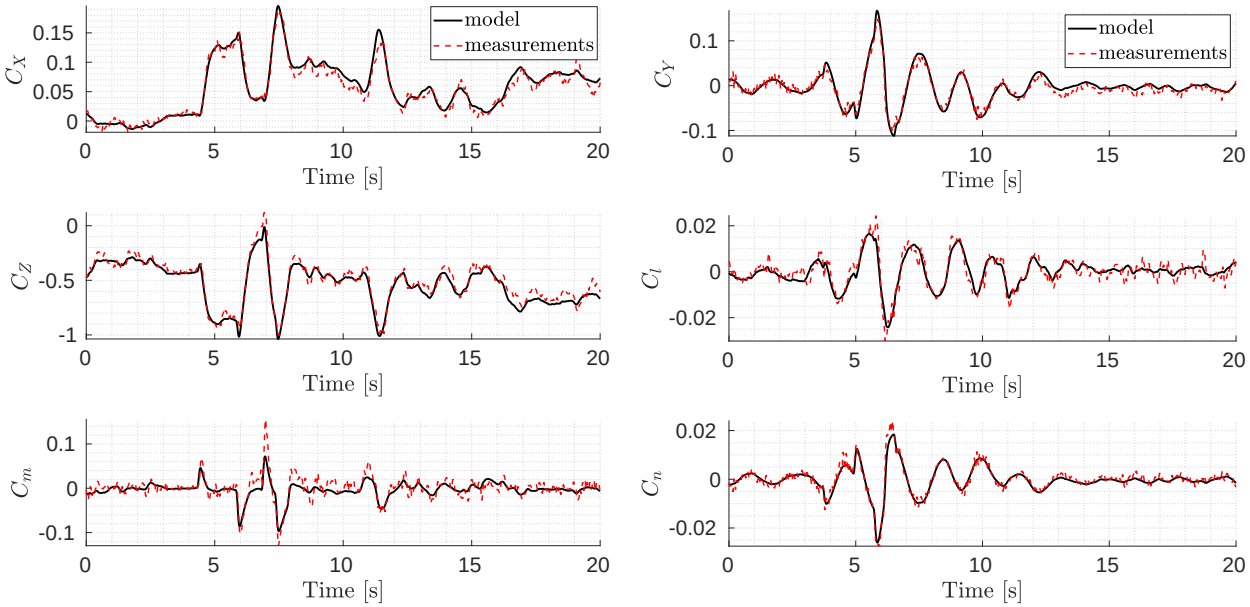

(a) 3211-input on the elevator **(b) 3211-input on the rudder**

Fig. 12 Simulation of two maneuvers flown during the tests using the estimated aerodynamic model

D. Comparison with wind-tunnel tests

The model predictions are compared to the existing static model from wind-tunnel data presented in Ref. [8]. The wind-tunnel data comes from a "clean" half wing of the same size and geometry as the free-flight test article of the present study. Differences should be expected to arise due to the wind-tunnel test article not having a landing gear (which was deployed at all times during the flight tests), engines and winglets. In addition, the lower surface of the free-flight test article has four holes for cooling and another one for the nose gear retraction. Finally, a zig-zag transition strip was applied to the leading-edge of the wind-tunnel test article, whereas on the free-flight test article only a carborundum strip was applied from the kink to the wingtip. A key aspect of the half-model is the small gap at the wall of the tunnel through which there is pressure communication. Moreover, the boundary layer of the tunnel interacts with the root of this half-model, introducing a lower loading on the front part of the model, as well as the formation of a root vortex. These fundamental flow structures are not present in the flight test, and these affect the slope of the pitching moment curve, the induced drag, and the lift coefficient. The comparison therefore should be interpreted with care.

In Fig. 13 the lift and pitching moment curves are compared between the flight test and the wind tunnel test. It can be seen how the lift slope identified from flight tests is considerably higher than that from the uncorrected wind-tunnel tests. Since the results of Ref. [8] have not been corrected for wind tunnel effects, the following wind tunnel corrections have been applied to the measurement data: a lift interference correction that changes the angle of attack and the drag coefficient, and a streamline curvature correction which affects the angle of attack and the pitching moment coefficient [49, 50]. The assumptions and calculations concerning the wind tunnel corrections can be found in Ref. [34]. The application of the wind tunnel corrections improves the correlation between the two experimental results significantly for the lift coefficient, whereas the discrepancies in the drag and pitching moment coefficients remain. However, it must be noted that the empirical corrections of Refs.[49, 50] have been derived for more conventional wing planform shapes. It is therefore understandable that there is still discrepancy between the results from the free-flight experiment and the wind-tunnel experiment.

The effects of the implementation of a winglet to the wind tunnel half model were investigated in Ref. [10], where it was found that the winglets neither increased the lift slope nor the zero-angle-of-attack lift coefficient. For this reason, the difference in zero-angle-of-attack lift coefficient is still under study, and it is thought that it could arise from an systematic offset in the angle-of-attack measurements.

Appreciable differences are found for the drag coefficient. This can be partly explained by the additional landing gear drag in flight, which increases the friction drag. However also a lower induced drag was found for the flight-test model, which at first sight could be attributed to the effect of the winglets. However, Johnson [10] showed that the winglet implementation does not lead to a reduction of the induced drag as it is commonly expected, so the difference in induced drag remains under study.

The pitching moment from the flight test shows a constant shift with respect to the wind tunnel results. This can again be explained by the landing gear drag in flight as it provides a negative (stabilizing) pitching moment. On the other hand, the pitching moment slope from flight tests and wind-tunnel tests seem to agree.

Finally, it should also be noted that the drag and pitching moment coefficients are more sensitive to inaccuracies in the engine modeling, which could also be the reason for some of the observed differences. Further wind-tunnel tests including engine and landing gear are planned in order to investigate the discrepancies found to date.

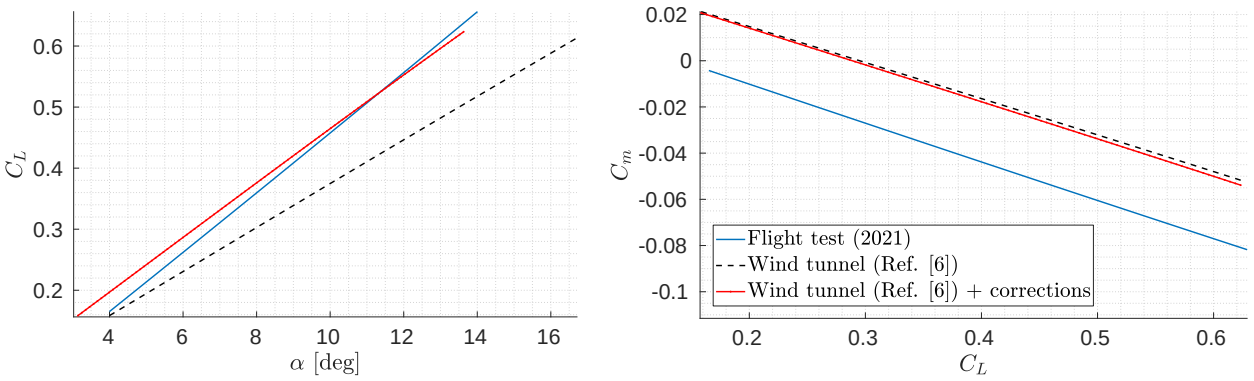

Fig. 13 Lift and pitching moment coefficients for the identified aerodynamic model and the wind tunnel results from a clean half wing from Ref. [8], with and without wind-tunnel corrections

VI. Flight Mechanics Analysis

A brief analysis from the flight mechanics point of view is presented here, consisting of an inspection of the aerodynamic derivatives and the calculation of the aircraft dynamic modes. The examination of the values of the estimated aerodynamic derivatives can offer good insight into the aircraft's static and dynamic response, which is summarized as follows and is in line with the experiences of the pilot during these flight tests:

- The aircraft longitudinal motions are statically and dynamically stable from the negative values of $C_{m\alpha}$ and $C_{m\hat{q}}$ respectively for the tested location for the center of gravity.
- The aircraft is directionally stable in static conditions from the positive value of $C_{n\beta}$
- Most of the derivatives have the same sign as in conventional tube-and-wing aircraft. For instance, there is a negative dihedral effect ($C_{l\beta}$) which arises from the positive dihedral angle and the backward sweep. The roll damping derivative ($C_{l\hat{p}}$) is also negative, with the main contribution coming from the antisymmetric lift distribution appearing in the wing with a roll rate. The yaw damping derivative ($C_{n\hat{r}}$) is again negative, as the main contribution is due to the antisymmetric drag distribution which appears on a wing with a yaw rate.
- $C_{Y\hat{p}}$ seems to be negligible for the Flying V since the main contribution to it comes from vertical surfaces. The only ones present are the winglets, which are small compared to the wing and close to the center of gravity, so the induced velocities on the winglets due to pitch rate will be small as well.
- $C_{Y\delta_a}$ is not negligible, which is sometimes the case for conventional aircraft. Instead, the ailerons generate lateral forces comparable to those from the rudders. The reason could be the short distance

between the elevons and the winglets [39].

- $C_{n\hat{p}}$ is negative, which is the opposite as in conventional aircraft and an unexpected result. The roll rate creates an antisymmetric induced drag distribution which in first approximation should generate a positive yawing moment. The contribution from vertical surfaces is proportional to $C_{Y\hat{p}}$ which is negligible as discussed above. The reason for the negative value of this derivative is still unknown.
- $C_{n\delta_a}$ is negative, which is a detrimental effect known as *adverse yaw* that worsens the handling during turns. Differential aileron deflection was already used during the tests, so a larger difference between up and down aileron deflection is needed.

Continuing, the aircraft dynamic modes determine the dynamic stability with respect to small perturbations from a reference flight condition (steady level flight). To calculate the dynamic modes, trim points are first found by implementing the identified aerodynamic model in a nonlinear flight mechanics simulation and looking for control combinations that result in equilibrium points. The model is linearized around these trim points and a state-space model is built. This allows the identification of the aircraft modes by finding the eigenvalues of the state transition matrix. The calculated modes for the airspeeds flown during the flight tests are shown in Fig. 14, which resembles the modes from a conventional aircraft. The longitudinal modes (short period and phugoid) are both stable except for the lowest speeds, where the phugoid enters the unstable region. The Dutch roll mode is stable but lightly damped, which was already observed during the flight tests and warranted the use of a yaw damper to improve the handling. A quick stable roll subsidence mode is also found, whereas the spiral is a very slow mode which is unstable at low speeds and becomes stable at higher speeds.

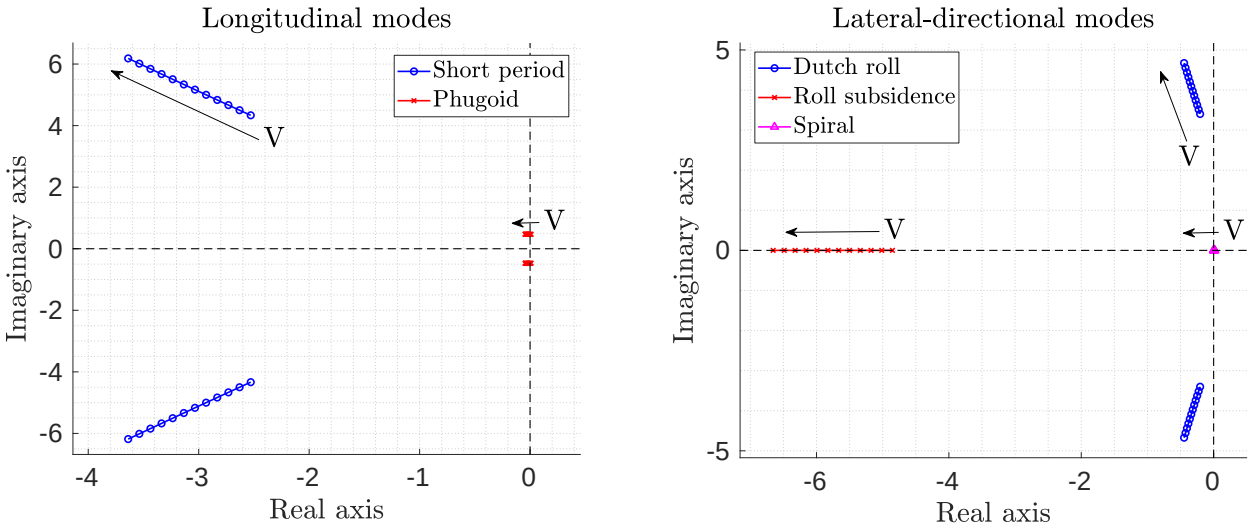

Fig. 14 Longitudinal and lateral-directional modes of the 4.6%-scale Flying V for $V \in [25, 36]$ m/s

VII. Conclusions

An aerodynamic model for the "Flying V" has been estimated using flight test data from a 4.6% sub-scale test article. The Two-Step method was applied in the context of scaled flight testing to decouple the state estimation and parameter estimation problems. An Iterated Extended Kalman Filter was able to adequately solve the state estimation problem, which included the estimation of sensor biases, wind speeds, and the upwash coefficient at the 5 hole pitot probe location. With regard to the parameter estimation, the dependencies of the aerodynamic coefficients were found using a stepwise regression technique, resulting on parsimonious models which only contain significant regressors. The models were validated using a subset of the gathered data not used for the estimation. Good prediction capabilities and reasonably uncorrelated residuals were found. The model fit to the data is adequate, attaining a relative RMS for the validation dataset below 7% for C_X, C_Y, C_Z and C_n, and below 10% for C_l and C_m. In addition, a good agreement was

found between the estimated lift coefficient and previous wind-tunnel results, whereas the pitching moment coefficient shows larger discrepancies, mainly because of the differences between the test articles. The aircraft dynamic modes were calculated using the estimated model and are consistent with the observations of the pilot, which reinforce the idea that the model is representative of the aircraft aerodynamic characteristics. Further investigations in the wind tunnel or in sub-scale flight tests are needed to determine the source of the existing discrepancies in an unambiguous way.

The main limitations of the aerodynamic model arise from the data used for the regression. A slow step-by-step approach was required during the flight tests in order to ensure the safety of the operation, and only a limited number of maneuvers were executed during each flight because of the available flight time. For this reason the first step to improve the model is to extend the dataset with more flights containing different maneuvers and flight conditions. It should be noted that even though the commanded maneuvers generated very useful data, a more careful maneuver design can be done now that an aerodynamic model is available, as the the maneuver periods and magnitudes can be adjusted to properly excite the aircraft dynamic modes.

In summary, the estimated aerodynamic model provides a simple set of analytical expressions that describe the aerodynamics of the Flying V, and which can be readily implemented in a flight simulator or used to design an optimal flight controller. It is noted that this relatively small dataset already highlights possible areas of improvement for the aerodynamic design of the aircraft. Further investigations will include the interpretation of these results from a sub-scale model for the flight dynamics of the full-scale model at higher Reynolds and Mach numbers.

Acknowledgements

The design, building and testing of the 4.6% test article was performed by the authors with the help of multiple colleagues. We would like to thank Fred Bosch, Victor Horbowiec, and Frank van Wissen for their contribution to the manufacturing of the airframe. Furthermore, we would like to thank Jan-Willem Kuijpers for his contribution to the flight control electronics and Lucas Rousselot for the manufacturing of the transportation jig. We would like to extend a special thank you to Gunnar Haase and Detlev Konigorski of Airbus GmbH for facilitating the flight test campaigns. Finally, we thank KLM Royal Dutch Airlines for their financial support for this project. Without their support, this project would not have been possible.

References

[1] Benad, J., "The Flying V - A new aircraft configuration for commercial passenger transport," *Deutscher Luft-und Raumfahrtkongress*, 2015.

[2] Faggiano, F., Vos, R., Baan, M., and van Dijk, R., "Aerodynamic Design of a Flying V Aircraft," *17th AIAA Aviation Technology, Integration and Operations Conference*, American Institute of Aeronautics and Astronautics, 2017.

[3] van der Schaft, L., "Development, Model Generation and Analysis of a Flying V Structure Concept," Master's thesis, Delft University of Technology, 2017.

[4] Claeys, M., "Flying V and Reference Aircraft Structural Analysis and Mass Comparison," Msc. thesis, Delft University of Technology, 2018.

[5] Rubio Pascual, B., and Vos, R., "The Effect of Engine Location on the Aerodynamic Efficiency of a Flying-V Aircraft," *AIAA Scitech 2020 Forum*, Orlando, FL, 2020. https://doi.org/10.2514/6.2020-1954.

[6] Oosterom, W., "Flying V Family Design," Msc. thesis, Delft University of Technology, 2020.

[7] Palermo, M., and Vos, R., "Experimental Aerodynamic Analysis of a 4.6%-Scale Flying-V Subsonic Transport," *AIAA Scitech 2020 Forum*, Orlando, FL, 2020. https://doi.org/10.2514/6.2020-2228.

[8] Ruiz García, A., Vos, R., and de Visser, C., "Aerodynamic Model Identification of the Flying V from Wind Tunnel Data," *AIAA AVIATION 2020 FORUM*, 2020. https://doi.org/10.2514/6.2020-2739.

[9] Empelen, S. V., and Vos, R., "Effect of Engine Integration on a 4.6%-Scale Flying-V Subsonic Transport," *AIAA Scitech 2021 Forum*, 2020. https://doi.org/10.2514/6.2021-0939.

[10] Johnson, N., "Effect of Winglet Integration and Rudder Deflection on Flying-V Aerodynamic Characteristics," Master's thesis, Delft University of Technology, 2021.

[11] van Uitert, J., "Experimental Investigation into the Effect of Aerodynamic Add-ons on the Aerodynamic Characteristics of the Flying V," Master's thesis, Delft University of Technology, 2021.

[12] Laban, M., "Online Aerodynamic Model Identification," Ph.D. thesis, Delft University of Technology, 1994.

[13] Klein, V., "Estimation of Aircraft Aerodynamic Parameters From Flight Data," *Progress in Aerospace Sciences*, Vol. 26, No. 1, 1989, pp. 1–77.

[14] Iliff, K. W., "Parameter Estimation for Flight Vehicles," *Journal of Guidance*, Vol. 12, No. 5, 1989, pp. 609–622.

[15] Hamel, P. G., and Jategaonkar, R. V., "Evolution of Flight Vehicle System Identification," *Journal of Aircraft*, Vol. 33, No. 1, 1996, pp. 9–28.

[16] Maine, R. E., and Iliff, K. W., "Formulation and implementation of a Practical Algorithm for Parameter Estimation with Process and Measurement Noise," *SIAM Journal of Applied Mathematics*, Vol. 41, No. 3, 1981, pp. 558–579. https://doi.org/10.1016/j.jfranklin.2011.05.010.

[17] Klein, V., Batterson, J. G., and Murphy, P. C., "Airplane Model Structure Determination from Flight Data," *Journal of Aircraft*, Vol. 20, No. 5, 1983, pp. 469–474.

[18] Gerlach, O., "Determination of Performance and Stability Parameters from Nonsteady Flight Test Maneuvers," *SAE Technical Paper*, , No. 700236, 1970.

[19] Mulder, J. A., "Design and evaluation of dynamic flight test manoeuvres," Ph.D. thesis, Delft University of Technology, 1986.

[20] de Visser, C. C., Mulder, J. A., and Chu, Q. P., "A Multidimensional Spline Based Global Nonlinear Aerodynamic Model for the Cessna Citation II," *AIAA Atmospheric Flight Mechanics Conference*, American Institute of Aeronautics and Astronautics, 2010.

[21] van den Hoek, M., de Visser, C. C., and Pool, D., "Identification of a Cessna Citation II Model Based on Flight Test Data," *4th CEAS Specialist Conference on Guidance, Navigation and Control*, 2017.

[22] Klein, V., and Batterson, J. G., "Aerodynamic parameters estimated from flight and wind tunnel data," *Journal of Aircraft*, Vol. 23, No. 4, 1986, pp. 306–312. https://doi.org/10.2514/3.45304.

[23] Klein, V.; Batterson, J. G., "Determination of Airplane Model Structure From Flight Data Using Splines and Stepwise Regression," NASA Technical Paper 2126, National Aeronautics and Space Administration, March 1983. https://doi.org/10.1007/978-90-481-9482-7.

[24] Klein, V., Batterson, J., and Smith, P., "On the Determination of Airplane Model Structure From Flight Data," *IFAC Identification and System Parameter Estimation*, Vol. 15, 1982, pp. 1163–1168. https://doi.org/10.1016/s1474-6670(17)63154-9.

[25] Batterson, J., G., and Klein, V., "Partitioning of flight data for aerodynamic modeling of aircraft at high angles of attack," *Journal of Aircraft*, Vol. 26, No. 4, 1989, pp. 334–339. https://doi.org/10.2514/3.45765.

[26] Ulbrich, N., "Regression Model Optimization for the Analysis of Experimental Data," *47th AIAA Aerospace Sciences Meeting including The New Horizons Forum and Aerospace Exposition*, 2009.

[27] Ulbrich, N., "Analysis of Multivariate Experimental Data Using A Simplified Regression Model Search Algorithm," *AIAA Ground Testing Conference*, 2013.

[28] Smith, P. L., "Curve Fitting and Modeling with Splines using Statistical Variable Selection Techniques," NASA Contractor Report 166034, National Aeronautics and Space Administration, 1982.

[29] Bruce, P., and Kellet, M., "Modelling and identification of non-linear aerodynamic functions using B-splines," *Proceedings of the Institution of Mechanical Engineers, Part G: Journal of Aerospace Engineering*, Vol. 214, 2000, pp. 27–40.

[30] de Visser, C. C., "Global Nonlinear Model Identification with Multivariate Splines - Application to Aerodynamic Model Identification of the Cessna Citation II," Ph.D. thesis, Delft University of Technology, 2011.

[31] Jategaonkar, R. V., "Flight Vehicle System Identification: A Time Domain Methodology," *Progress in Aeronautics and Astronautics*, Vol. 216, 2006.

[32] Wolowicz, C. H., Bowman-Jr, J. S., and Gilbert, W. P., "Similitude requirements and scaling relationships as applied to model testing," NASA Technical Paper 1435, National Aeronautics and Space Administration, 1979.

[33] Gonzalez, R., and Dabove, P., "Performance Assessment of an Ultra Low-Cost Inertial Measurement Unit for Ground Vehicle Navigation," *Sensors*, Vol. 19, No. 18, 2019. https://doi.org/10.3390/s19183865.

[34] Ruiz García, A., "Aerodynamic Model Identification of the Flying V using Wind Tunnel Data," Msc. thesis, Delft University of Technology, 2020.

[35] Kraus, F., Qiu, X., and Schaufelberger, W., "Identification and control of a servo systems," *IFAC Proceedings Volumes*, Vol. 30, 2017, pp. 197–202.

[36] Mulder, J. A., Chu, Q. P., Sridhar, J. K., Breeman, J. H., and Laban, M., "Non-linear aircraft flight path reconstruction review and new advances," *Progress in Aerospace Sciences*, Vol. 35, No. 7, 1999, pp. 673–726. https://doi.org/10.1016/S0376-0421(99)00005-6.

[37] Mulder, J. A., Chu, Q. P., Sridhar, J. K., Breeman, J. H., and Laban, M., "Non-linear aircraft flight path reconstruction review and new advances," *Progress in Aerospace Sciences*, Vol. 35, No. 7, 1999, pp. 673–726. https://doi.org/10.1016/S0376-0421(99)00005-6.

[38] De Visser, C. C., "Global Nonlinear Model Identification with Multivariate Splines," Ph.D. thesis, Delft University of Technology, 07 2011.

[39] Gómez-Tierno, M. A., Pérez-Cortés, M., and Puentes-Márquez, C., *Mecánica del Vuelo*, 2nd ed., Garceta Grupo Editorial, 2012.

[40] Morelli, E. A., "Practical Aspects of the Equation-Error Method for Aircraft Parameter Estimation," *AIAA Atmospheric Flight Mechanics Conference and Exhibit*, American Institute of Aeronautics and Astronautics, 2006, pp. 1–18. https://doi.org/doi:10.2514/6.2006-6144.

[41] Mithra, S. K., and Rao, C. R., "Conditions for Optimality and Validity of Simple Least Squares Theory," *The Annals of Mathematical Statistics*, Vol. 40, No. 5, 1969, pp. 1617–1624.

[42] Hsia, T. C., *System Identification*, Lexington Books, 1977.

[43] Montgomery, D. C., Peck, E. A., and Vining, G. G., *Introduction to Linear Regression Analysis*, 5th ed., Wiley Series in Probability and Statistics, Wiley, 2012.

[44] Klein, V., and Morelli, E. A., *Aircraft System Identification: Theory and Practice*, American Institute of Aeronautics and Astronautics, 2006.

[45] Morelli, E. A., and Klein, V., "Accuracy of Aerodynamic Model Parameters Estimated from Flight Test Data," *Journal of Guidance, Control, and Dynamics*, Vol. 20, No. 1, 1997.

[46] Montgomery, D. C., *Design and Analysis of Experiments*, 7th ed., John Wiley & Sons, 2009.

[47] Morelli, E. A., "Global Nonlinear Aerodynamic Model Using Multivariate Orthogonal Functions," *Journal of Aircraft*, Vol. 32, No. 2, 1995, pp. 270–277.

[48] van Arnhem, N., de Vries, R., Sinnige, T., Vos, R., Eitelberg, G., and Veldhuis, L. L., "Engineering method to estimate the blade loading of propellers in nonuniform flow," *AIAA Journal*, Vol. 58, No. 12, 2020, pp. 5332–5346.

[49] Barlow, J. B., H. Rae, W. J., and Pope, A., *Low-Speed Wind Tunnel Testing*, 3rd ed., Wiley, 1999.

[50] Acum, W., Garner, H., Maskell, E., and Rogers, E., AGARD Technical Report 109, AGARD, 1986.